The Thesis Committee for Stephen Yin-Chyuan Jong
Certifies that this is the approved version of the following thesis:

Investigating the Impact of Salinity Gradient Design on Low Tension Gas Flooding Performance

APPROVED BY
SUPERVISING COMMITTEE:

Supervisor: _____
Quoc P. Nguyen

Co-Supervisor: _____
Kishore Mohanty

Investigating the Impact of Salinity Gradient Design on Low Tension Gas Flooding Performance

by

Stephen Yin-Chyuan Jong

Thesis

Presented to the Faculty of the Graduate School of

The University of Texas at Austin

in Partial Fulfillment

of the Requirements

for the Degree of

Master of Science in Engineering

The University of Texas at Austin

May 2018

Dedication

To those for whom this work was not in vain, my loving wife and unborn child, my supportive parents and my caring siblings, and to my God, the Father of my Lord Jesus Christ, who is above all I give my heartfelt thanks and remembrance.

Abstract

Investigating the Impact of Salinity Gradient Design on Low Tension Gas Flooding Performance

Stephen Yin-Chyuan Jong, M.S.E

The University of Texas at Austin, 2018

Supervisor: Quoc P. Nguyen

Co-Supervisor: Kishore Mohanty

Low Tension Gas (LTG) flooding is an emerging chemical enhanced oil recovery (EOR) process analogous to Surfactant-Polymer (SP) flooding but replaces polymer with aqueous foam for liquid mobility control to extend application to high salinity, high temperature, and low permeability reservoirs. Several authors have already investigated LTG application in these challenging conditions, but with limited insight into the impact of salinity gradient design on LTG performance.

A combination coreflooding and modeling-simulation study using a newly-developed LTG model revealed that altering salinity gradient could result in up to 15% improvement in residual oil recovery in moderate permeability sandstone through improved mobility control and reduced dispersive mixing and also demonstrated the importance of describing microemulsion-foam interactions. A follow-up study using realistic porous media microfluidics shed light on the correlation between microemulsion phase behavior and foam stability, with a 90%

decrease in foam stability with increasing salinity within the Winsor Type I region alone.

These studies together highlighted the tradeoff between low interfacial tension microemulsion phase behavior for oil mobilization and foam stability for liquid mobility control and oil displacement and also indicated that alternative salinity gradients to optimum salinity slug injection should be investigated on a problem-specific basis. In particular cases, foam mobility control may be more important than microemulsion phase behavior and *vice versa*. Furthermore, results from both studies showed a strong need for a mechanistic model for dynamic gas trapping in the presence of foam and provided motivation for future experimental and modeling work concerning this phenomenon.

Table of Contents

Chapter 1: Introduction

1.1 Overview

Low Tension Gas flooding is a chemical EOR process which employs surfactant to generate low interfacial tension microemulsions to mobilize residual oil and generate and propagate foams to provide liquid mobility control and displace mobilized oil. LTG is a close analogue to SP flooding, with the key difference being the co-injection of gas to form aqueous foams for liquid mobility control in the LTG process compared to aqueous polymer solution in the SP process. Due to this substitution, LTG applicability extends even to technically and economically challenging reservoir conditions such as high salinity, high temperature, and low permeability.

Microemulsion phase behavior and surfactant transport are key to surfactant flooding success and are primarily determined by the electrolyte concentration, although several other contributing factors exist as well. Traditional surfactant flooding relies on a negative salinity gradient involving chemical slug injection at optimum salinity and drive injection in the Winsor Type I regime. Previous pioneering LTG studies have focused on determining the effects of other factors while adopting the traditional negative salinity gradient of SP flooding. However, these studies have not taken into account the potential of microemulsion-foam interactions. If microemulsion phase behavior and foam mobility control have significant interactions, then optimal salinity gradient design for LTG flooding will require unique considerations and may not conform to traditional salinity gradient design criteria for SP flooding.

1.2 Research Objectives and Methodology

1.2.1 Objectives

These are the main objectives of this work:

1. Develop and implement an LTG model in CMG GEM to improve coreflood performance analysis and provide additional insight into the LTG process.
2. Investigate the impact of salinity gradient on LTG flooding performance and determine the significance of microemulsion-foam interactions.
3. Quantify and explain the interaction between microemulsion phase behavior and foam stability if the interaction is deemed to be significant.

1.2.2 Methodology

An extensive literature review was first performed to relevant foam and microemulsion knowledge as well as existing work concerning salinity gradient and the LTG process in order to assess the current state of knowledge and identify gaps in understanding. In addition, microemulsion and foam modeling were reviewed in preparation for the development of a new LTG model for application to this study.

LTG coreflooding experiments with moderate permeability Berea sandstone were performed with two different salinity gradients to assess the impact of salinity gradient on LTG performance and the significance of microemulsion-foam interactions while also providing model validation. Oil recovery, oil cut, sectional pressure drop, effluent conductivity, and pure vs. emulsified oil production were recorded to quantify performance and provide a set of data for comparison between cases.

The simulation study with the newly-developed LTG model incorporated experimental data for model calibration in order to reduce the parameter space and resulting uncertainty and involved simultaneous matching of cumulative oil recovery and pressure drop data. Deviations between experimental and simulation data were examined to determine if the source was experimental error or the inability of the simulator to describe the experimental phenomena. Matched simulation parameters were paired with experimental data to examine the impact of varying salinity gradient and determine the mechanisms responsible for explaining the differences. Particular attention was paid to the significance of microemulsion-foam interactions.

In order to further quantify and explain the interaction between microemulsion phase behavior and foam stability, an experimental study was performed to quantify foam stability in the presence of microemulsion at various electrolyte concentrations in both bulk and porous media foam using realistic porous media microfluidic chips.

Chapter 2: Literature Review

2.1 Low Tension Gas Flooding

The LTG process is an alternative to ASP flooding for challenging reservoir conditions such as high salinity, high temperature, and low permeability (Srivastava 2009, Szlendak 2013) and relies on surfactant injected either concurrently (co-injection) or alternatively with gas to form aqueous foams *in-situ* to provide liquid mobility control for the chemical slug, which generates low interfacial tension microemulsion for oil mobilization. Whereas these challenging conditions lead to prohibitive costs for polymer implementation both in terms of chemicals and facilities costs, foam mobility control requires only a source of gas (typically CO_2, N_2, or hydrocarbon gas). In addition, some gases may either develop partial or complete miscibility with oil or favorable oil displacement characteristics under certain reservoir conditions. This may lead to synergistic behavior in combination with the injected surfactant and/or reduce the need for high performance surfactant, although this potential benefit has not yet been well-studied.

Furthermore, foam has the benefit of providing enhanced mobility reduction in higher permeability media compared to lower permeability media, which enables diversion of injected liquids from higher permeability to lower permeability channels that would otherwise be bypassed (Nguyen 2009).

2.2 Aqueous Foams for Liquid Mobility Control

2.2.1 Background

Aqueous foams are thermodynamically unstable dispersions of gas in water and are characterized by discrete gas bubbles separated by thin liquid films called

lamellae (Schramm 1994). These foams have been traditionally employed to improve sweep efficiency in gas and steam flooding processes by reducing the mobility of injected gas and steam and diverting flow to otherwise uncontacted oil (Green and Willhite 1998). However, aqueous foams have recently received increased attention due to their excellent liquid mobility control potential for chemical EOR processes such as LTG flooding.

2.2.2 Foam Generation

Foam may be generated by capillary snap-off, lamella division, or leave-behind mechanisms. While snap-off appears to be responsible for generation of initial films (Kovscek and Radke 1993), this mechanism requires a large amount of liquid and is most likely not responsible for additional generation of secondary films. Instead, lamella division is probably responsible for generation of additional films (Kam *et al.* 2004). Leave-behind may be more dominant if the foam is especially high quality (high fraction of gas).

2.2.3 Kinetics of Foam Drainage

Foam is not inherently stable and thus undergoes destruction via film rupture as the film drains and thins beyond a critical thickness. Drainage occurs due to two main mechanisms: gravity drainage and capillary suction (Chambers and Radke 1991).

Capillary suction arises from the fact that the lamellae are flat in the center but curve outwards at the ends. This results in a higher pressure at the center and lower pressure at the plateau borders, which leads to fluid naturally draining from the film due to the pressure difference. As the film thins, it approaches a critical

capillary pressure at which it will rupture. This critical thickness/pressure depends strongly on the surfactant formulation (Derjaguin and Obukhov 1936, 1939).

Both capillary suction and gravity drainage are mitigated by increasing bulk and surface viscosity, which will reduce the drainage rate. In addition, there are natural forces which act at the film interface to determine foam stability. On either side of the thin liquid film there are electrical charges due to an electrical double layer and aggregated ionic surfactants. This leads to repulsive forces that depend on charge density and film thickness and are described by the following expression:

$$V_R = V_1 \exp\left(-\kappa t\right) \quad (2.1)$$

Induced dipole-dipole forces represent the most significant attractive force and are quantified by the following expression:

$$V_A = -\frac{V_2}{t^2} \quad (2.2)$$

The sum of these forces is known as the interaction energy, which is given below:

$$V = V_R + V_A = \left[V_1 \exp\left(-\kappa t\right)\right] - \frac{V_1}{t^2} \quad (2.3)$$

Derjaguin and Landau (1941) and Verwey and Overbeek (1948) developed what is known as DLVO theory, which takes the derivative of the total interaction energy to obtain the disjoining pressure:

$$\pi\left(t\right) = -\frac{dV}{dt} \quad (2.4)$$

This disjoining pressure represents the amount of pressure that must be applied to the liquid film in order to maintain a certain film thickness, or the net force that resists drainage. The disjoining pressure must be positive in order to balance capillary forces.

At low surfactant concentrations (well below CMC), the Gibbs-Marangoni effect arises due to the induced surface-tension gradient. Surfactant flows to the plateau borders due to bulk flow and the relatively higher concentration at the borders creates an IFT contrast between the center of the film and the outer portion. Liquid will flow from the low to high IFT region, thus resisting flow out of the film. In addition, increasing the viscosity of the bulk liquid will also retard film thinning.

The ability of a liquid surface to adjust its surface tension to an instantaneous stress is known as its dilatational modulus. A higher dilatational modulus means that surface tension gradients are developed more readily and thus the film will be more elastic and stable. This dilatational modulus is a function of surfactant type and concentration.

However, at higher surfactant concentrations well above the CMC where typical foam processes are carried out, micelles form and become organized, which increases the pressure of the aqueous film beyond that in the bulk aqueous phase. This excess pressure is called structural disjoining pressure and is caused by micellar structuring when confined in an aqueous film. Micellar structuring has been demonstrated to result in delayed film thinning in a stepwise manner.

2.2.4 Foam-Oil Interactions

Foam stability is also affected by the presence of crude oil (Wasan *et al.* 1988), and numerous authors have attempted to qualify and quantify foam-crude oil interactions via various theoretical models. However, none of the existing models is able to consistently explain the impact of crude oil on foam stability for every given surfactant-oil-water system.

However, the work of Nikolov (1986), who sonicated oil to form droplets before introducing them to foam films and measuring subsequent stability against droplet size and concentration, laid the foundation for considering the impact of emulsified oil on foam stability instead of bulk oil effects. Theory and experimental work indicate that oil-swollen micelles may affect micellar structuring and decrease foam stability compared to oil-free micelles due to reduced intramicellar repulsion. This is particularly relevant for the LTG process operating in tertiary recovery mode, in which oil is at residual saturation to water flooding and flowing channels are fully occupied by water. Furthermore, the microemulsions generated during the LTG process are comprised of micelles which may impact the stability of generated foams.

Preliminary work by Srivastava (2010) on bulk foam and sandpack foam stability using microemulsions indicated that Type II microemulsions were the least beneficial to foam stability, Type I microemulsion were the most beneficial to foam stability, and Type III microemulsions were somewhere in between.

2.2.5 Foam Mobility in Porous Media

Aqueous foams are not thermodynamically stable and thus cannot be treated as a pure phase, but their impact is typically represented as altering existing gas mobility (i.e. gas mobility in the presence of foam). Therefore, Darcy's

Law may be applied to describe the mobility of gas in the presence of foam, yielding both an apparent viscosity and a relative permeability.

2.2.5.1 Foam Apparent Viscosity

Foam has been shown to be shear-thinning (Bretherton 1961), with effective viscosity varying inversely with bubble velocity raise to the 1/3 power. Hirasaki and Lawson (1985) extended the work of Bretherton and discovered that surface tension gradients caused by surfactants increase foam apparent viscosity significantly. In fact, neglecting surface tension gradients leads to underestimating the effective viscosity by a factor of eight.

2.2.5.2 Gas Trapping in the Presence of Foam

Foam has been shown to demonstrate yield-stress behavior, requiring a minimum mobilization pressure gradient to transport due to the resistance of individual lamellae to stretching. When the pressure gradient is below the minimum mobilization pressure gradient, gas is immobilized. Experimental work has shown gas trapping in the presence of foam to range from 50% to 99% of the total gas saturation (Radke and Gillis 1990, Friedmann *et al.* 1991, Tang and Kovscek 2006, Nguyen *et al.* 2009, Kil *et al.* 2011). Gas trapping in the presence of foam reduces the saturation of flowing gas and thus reduces the relative permeability of gas via relative permeability effects.

2.3 SURFACTANT ENHANCED OIL RECOVERY

2.3.1 Background

Surfactants, or surface-active agents, or molecules with a hydrophobic tail group and a hydrophilic head group that tend to aggregate at the interface between

two immiscible fluids. Surfactants that aggregate at the interface between oil and water and lower interfacial tension (IFT) are employed in surfactant EOR processes to improve displacement efficiency. Addition of surfactant to an oil-water system will result in lower IFT until the critical micelle concentration (CMC) is reached, after which the IFT will remain relatively constant and additional surfactant will contribute to the formation of micelles.

2.3.2 Microemulsion Phase Behavior

When surfactants are introduced to systems containing oil and water, a microemulsion phase may form provided that the surfactant concentration is above the CMC. A microemulsion is a thermodynamically stable and isotropic mixture of two immiscible liquids. The phase behavior of microemulsions is determined by a multitude of factors, most notably electrolyte concentration (*i.e.* salinity). At low salinities, a two-phase system prevails with oil solubilized within a water-rich Winsor Type I microemulsion phase that is in equilibrium with a pure excess oil phase. Conversely at high salinities, a two-phase system prevails with water solubilized within an oil-rich Winsor Type II microemulsion phase that is in equilibrium with a pure water phase. Between these two salinity extremes, a three-phase system prevails with oil and water solubilized within a middle-phase Winsor Type III microemulsion phase that is in equilibrium with pure oil and pure water.

Type III systems have two interfaces: oil-microemulsion and water-microemulsion, and the IFTs of these two interfaces move oppositely within the Type III salinity region (Fig. 2.1).

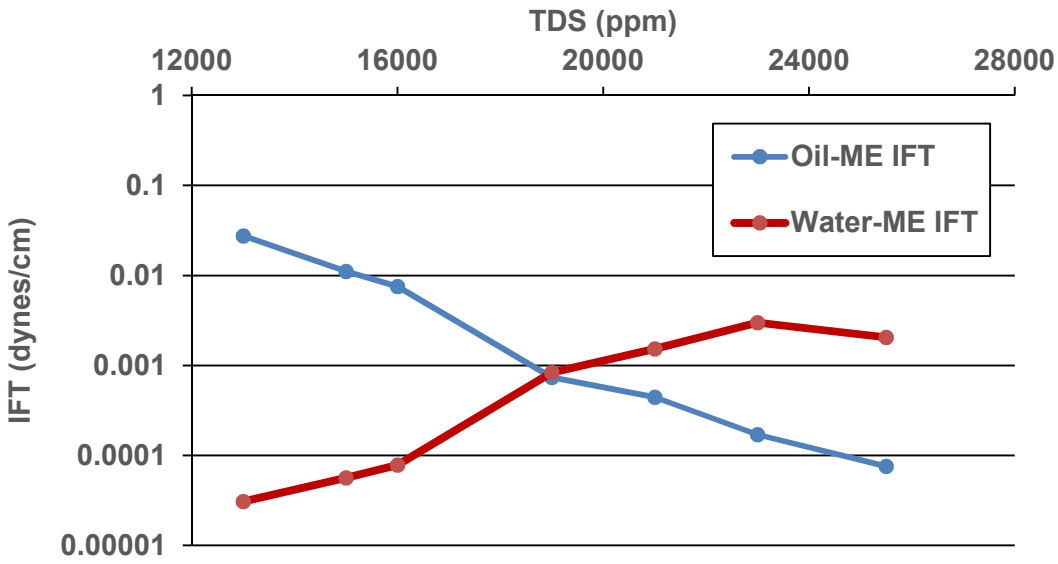

Figure 2.1: Oil-microemulsion and water-microemulsion interfacial tension vs. salinity.

Near the Type I boundary, the water-microemulsion IFT is at a minimum while oil-microemulsion IFT is at a maximum, and the water-microemulsion and oil-microemulsion IFTs increase and decrease with increasing salinity, respectively, until the Type II boundary, where oil-microemulsion IFT is at a minimum and water-microemulsion IFT is at a maximum.

Healy and Reed (1977) demonstrated that for a Type III environment with two interfaces, the higher IFT interface will dictate performance in a surfactant EOR process. This means that oil mobilization is maximized when both IFTs are equal, which is equivalent to the optimum salinity point described previously.

2.3.3 Salinity Gradient Design for Surfactant Flooding

Although oil mobilization is maximized under the low IFT conditions of optimum salinity, constant injection of high performance surfactant at optimum salinity is not economically viable. While Type III microemulsions exhibit ultralow IFT, they are also difficult to break at the surface due to their stability and make it costly to free oil that has been emulsified. Furthermore, the polymer chemicals which are often used to provide mobility control for surfactant floods tend to degrade in high salinity environments. Lastly, surfactant adsorption is also reduced with decreasing salinity (Noll and Gall 1991, Azam *et al.* 2013). Therefore, it is desirable to inject a finite slug solution at optimum salinity followed by a drive solution of the same or altered chemical composition in the Winsor Type I region (Nelson and Pope 1978, Hirasaki 1983).

Chapter 3: Development of LTG Model

Because the LTG process can be understood as the sum of microemulsion and foam processes with some interaction, LTG modeling may be split into microemulsion and foam modeling. Focus will be given here to state-of-the-art modeling that is also predominantly accepted as standard approach.

3.1 Model Development – Microemulsion

3.1.1 General Framework

The goal of surfactant flooding as a tertiary EOR method is to recover oil that is either physically or economically unrecoverable by other means. The amount of oil that may be recovered at any time is most simply determined by the capillary number, a dimensionless ratio of viscous to capillary forces (Delshad *et al.*1986). The capillary number shown in Eq. 3.1 is derived from a force balance on a trapped oil droplet surrounded by water and may also be extended to a trapping number to include gravity effects.

$$N_{Tl} = \frac{\left| -\vec{\vec{k}} \cdot \vec{\nabla}\Phi_{l'} - \vec{\vec{k}} \cdot \left[g\left(\rho_{l'} - \rho_{l}\right)\vec{\nabla}h \right] \right|}{\sigma_{ll'}} \quad (3.1)$$

The more viscous force is applied or the lower the capillary forces become, the higher the oil recovery or lower the residual (remaining) oil saturation should be. Typical reservoirs have residual oil saturations that are insensitive to capillary number at both the low and high range but experience a dramatic drop-off in an intermediate range beginning at what is known as the critical capillary number. This leads to a reverse S-shaped capillary desaturation curve (CDC).

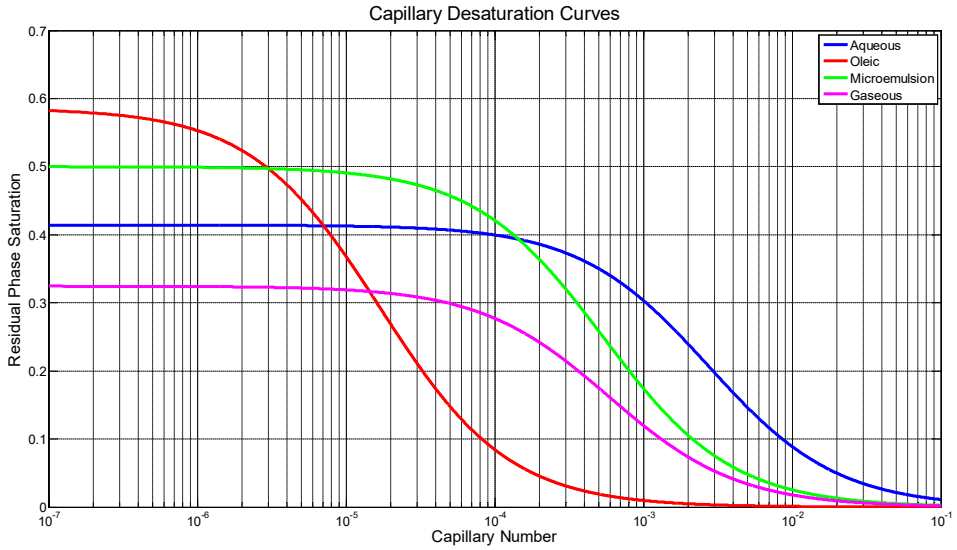

Fig. 3.1: Sample capillary desaturation curves for aqueous, oleic, microemulsion, and gaseous phases.

Secondary processes such as water flooding and polymer flooding do not provide practical means for moving past the low capillary number range, as they are only able to increase viscous forces by a relatively miniscule amount (Sheng 2011). However as mentioned previously, surfactant is capable of lowering the IFT between oil and water by several orders of magnitude, depending on microemulsion phase behavior.

This process and its end effects have been successfully modeled via the following framework:

1) Determine Phase Behavior
2) Calculate Solubilization Ratio(s)/Interfacial Tension(s)
3) Calculate Capillary Number(s)
4) Find New Residual Phase Saturations
5) Rescale Relative Permeability Curves

3.1.2 Mechanistic Microemulsion Model

This approach was first introduced with UTCHEM by Pope and Nelson (1978) in their paper describing the chemical flooding compositional simulator. UTCHEM employs a mechanistic microemulsion model backed by theory and experimental validation.

Microemulsion systems may be described by ternary diagram representations, in which the components are lumped into pseudocomponents: water, oil, and surfactant (Healy and Reed 1977). These three pseudocomponents are the corners of a triangle, within which all possible compositions of pseudocomponents lie. Traditionally, the surfactant pseudocomponent is at the top of the ternary diagram.

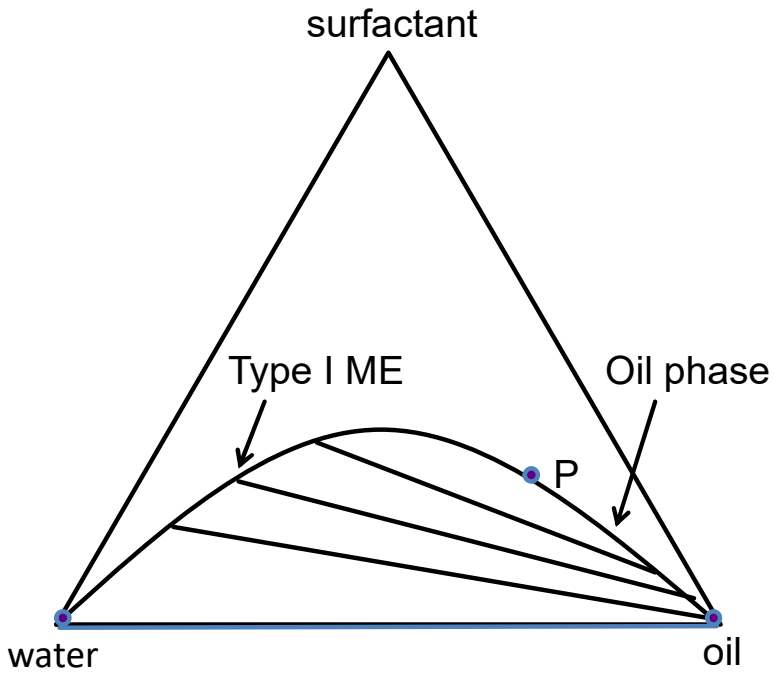

Fig 3.2: Sample ternary diagram for the Winsor Type I microemulsion regime.

A binodal curve on the ternary diagram represents the separation of single and multiphase regions. If a composition lies above the binodal curve then the system is single-phase; otherwise, the system will be multiphase (two or three phases). This binodal curve is determined experimentally and is unique for each surfactant system. It is possible for a system to deviate greatly from the standard-looking binodal curve (Green and Willhite 1998).

Tie lines are drawn between compositions on the binodal curve to show what equilibrium phase compositions each global composition will result in. These tie lines are also determined experimentally. Hand (1929) showed that a binodal curve and tie lines could be represented by relationships between equilibrium phase composition ratios, and Pope and Nelson (1978) extended that work to surfactant/oil/water systems.

$$\frac{C_{3l}}{C_{2l}} = A\left(\frac{C_{1l}}{C_{3l}}\right)^{\begin{matrix} l^{TypeI}=2,3 \\ l^{TypeII}=1,3 \end{matrix}} \quad (3.2a)$$

$$\frac{C_{3l}}{C_{2l}} = E\left(\frac{C_{33}}{C_{13}}\right)^{\begin{matrix} l^{TypeI}=2 \\ l^{TypeII}=1 \end{matrix}} \quad (3.2b)$$

C_{ij} is the concentration of component i in phase j. Water, oil, and surfactant are components 1, 2, and 3, respectively and aqueous, oleic, and microemulsion are phases 1, 2, and 3, respectively. A is a parameter related to the maximum height of the binodal curve and scales with salinity, while E depends on A and the composition at the plait point. The equilibrium compositions that are determined from phase behavior calculations may be used to calculate the solubilization ratio.

$$R_{l3} = \frac{C_{l3}}{C_{33}} \ (l = 1, 2) \ (3.3)$$

The solubilization ratios for oil and water are defined as the volume of oil per unit volume of surfactant in the microemulsion phase and the volume of water per unit volume of surfactant in the microemulsion phase, respectively. In a Winsor Type I/II environment only the oil/water solubilization ratio is necessary, while in a Winsor Type III environment, both oil and water solubilization ratios are necessary. Huh (1979) showed that these solubilization ratios could be correlated with the interfacial tension between two phases via the following general relationship:

$$\sigma_{l3} = \frac{c}{\left(R_{l3}\right)^2} \ (l = 1, 2) \ (3.4)$$

Once the interfacial tensions are calculated, capillary/trapping numbers are calculated via Eq. 3.4 above and used to determine new residual saturations via the CDC.

$$S_{lr} = \min\left(S_l, \left[S_{lr}\right]_H + \frac{\left[S_{lr}\right]_L - \left[S_{lr}\right]_H}{1 + T_l \cdot N_{T_l}} \right) (3.5)$$

The parameter T_l is a positive parameter that describes the CDC and N_{T_l} is the trapping number. $\left[S_{lr}\right]_L$ and $\left[S_{lr}\right]_H$ are the low capillary and high capillary number endpoints for residual phase saturation, respectively.

The Corey-type relative permeability endpoints and exponents are similarly interpolated between low and high values based on the residual saturation of the displacing phase. This relationship was first shown experimentally by Delshad (1986).

$$k_{rl}^{\circ} = \left[k_{rl}^{\circ}\right]_L + \frac{\left[S_{l'r}\right]_L - S_{l'r}}{\left[S_{l'r}\right]_L - \left[S_{l'r}\right]_H}\left(\left[k_{rl}^{\circ}\right]_H - \left[k_{rl}^{\circ}\right]_L\right) \ (l = 1,2,3) \quad (3.6)$$

$$n_l = \left[n_l\right]_L + \frac{\left[S_{l'r}\right]_L - S_{l'r}}{\left[S_{l'r}\right]_L - \left[S_{l'r}\right]_H}\left(\left[n_l\right]_H - \left[n_l\right]_L\right) \ (l = 1,2,3) \quad (3.7)$$

Even though this microemulsion model is fairly mechanistic, in practice certain data must be estimated instead of directly measured, which introduces empiricism into the approach. For instance, the binodal curve and tie lines are simplified by several assumptions and are typically back-calculated from experimental solubilization ratio data. In addition, the capillary desaturation curves for displaced/displacing phase pairs is not practical to measure and may either be used as a fitting parameter or replaced by one from the literature.

3.1.3 Streamlined Microemulsion Model

Considering that even the most mechanistic approaches introduce empiricism due to either computational complexity or limited availability of experimental data, a streamlined approach may be introduced that narrows down the process to key parameters which may be readily determined experimentally. This approach would retain the aforementioned framework and focus more on the end effects of the process rather than trying to model every aspect of the process in detail. Several assumptions may be made to simplify the modeling approach:

1. Winsor Type III microemulsion phase need not be modeled because:
    a. Transport of oil, water, and microemulsion in a Type III microemulsion phase environment is dominated by ultra-low IFT effects on relative permeability, as displacement of residual oil

comes overwhelmingly from decrease in capillary forces trapping oil rather than increased applied pressure gradient

b. Type III microemulsion viscosity should be minimized in an optimal chemical formulation to prevent phase trapping, thereby further reducing its impact on transport.

c. Large volume of Type III microemulsion is not desirable from an economic standpoint (more surfactant required, high processing costs for produced microemulsion) and does not yield additional benefit in mobilizing residual oil. Moreover, low concentration of surfactant (and minimal volume of Type III microemulsion) would reduce surfactant adsorption on the rock surface.

2. Oil-microemulsion and water-microemulsion interfaces in a true Type III environment may be condensed to one oil-water interface according to the principle of controlling IFT (Healy and Reed 1977), which states that the higher IFT between oil-microemulsion and water-microemulsion IFTs will dictate performance in a surfactant process. This in conjunction with the first assumption simplifies the microemulsion model from three phases to two phases, reducing complexity, uncertainty, and computational expense from four phase capillary desaturation and relative permeability.

The key output of microemulsion phase behavior is oil and water solubilization ratios which are routinely measured and related to interfacial tension by the Chun-Huh correlation.

Solubilization data is recorded in a table that is referenced and interpolated as a function of salinity, which is the main parameter controlling microemulsion

phase behavior for the LTG process. Two IFTs are calculated corresponding to the oil-microemulsion and water-microemulsion interfaces and the lower IFT is discarded per the principle of controlling IFT mentioned previously.

The surfactant component is partitioned between oil and water (Eq. 3.8) using a microemulsion composition weighting factor (Eq. 3.9) to reflect that the surfactant should transport according to the theoretical composition of the microemulsion phase.

$$V_{surf,oil} = k_s \cdot V_{surf,total} \quad (3.8a)$$

$$V_{surf,water} = \left(1 - k_s\right) \cdot V_{surf,total} \quad (3.8b)$$

$$k_s = \frac{V_{o,me}}{V_{o,me} + V_{w,me}} \quad (3.9)$$

The interfacial tension is used to calculate the capillary number according to Eq. 3.10:

$$N_c = \frac{k \nabla \Phi_w}{IFT_{avg}} \quad (3.10)$$
$$\Phi_w = P + \rho_w g h$$

Here k is the absolute permeability and $\nabla \Phi_w$ is the potential gradient across the oleic phase. Interpolation is then performed between three sets of relative permeability data corresponding to low, intermediate, and high capillary number data according to the following equation, which mimics the curvature of capillary desaturation data on a logarithmic plot:

$$F_{N_c} = \frac{\log N_c - \log N_{c,low}}{\log N_{c,high} - \log N_{c,low}} \quad (3.11)$$

$$RPV = F_{N_c}\left(RPV_{high}\right) + \left(1 - F_{N_c}\right)(RPV_{low}) \quad (3.12)$$

Here F_{N_c} is the logarithmic weighting parameter, RPV_{high} and RPV_{low} are high and low capillary number relative permeability values, respectively, and $N_{c,high}$ and $N_{c,low}$ are high and low capillary number limits, respectively. These values and limits depend on which set of two capillary number limits the current capillary number falls between. The assumptions previously made allow for the system to be reduced to one conjugate phase pair with a single capillary number with phase residual saturation, relative permeability endpoints, and relative permeability curvatures all being functions of capillary number.

The low capillary number data is best understood as relative permeability under waterflood conditions and the high capillary number data is the theoretical limit of miscible flooding conditions, i.e. straight-line relative permeability (Gupta 1979, Bardon and Longeron 1980, Harbert 1983, Ronde 1992). The intermediate capillary number data allows water and oil to desaturate independently based on capillary number, consistent with classical phase desaturation.

3.2 Model Development – Foam

The two most prevalent approaches to foam modeling are the population balance framework first introduced by Patzek (1988) and further developed by Kovscek *et al.* (1995) and the empirical foam model commonly implemented in the CMG STARS reservoir simulator.

3.2.2 Population Balance Approach

3.2.2.1 Foam Texture

The foundation for the population balance approach is a population balance on the mean bubble size:

$$\frac{\partial\left[\phi\left[S_f n_f + S_t n_t\right]\right]}{\partial t} + \frac{\partial\left(u_f n_f\right)}{\partial x} = \phi S_g\left(r_g - r_c\right) \quad (3.13)$$

S_f and S_t are the saturations of flowing and trapped gas, respectively. Likewise n_f and n_t are the flowing and trapped lamella densities, respectively u_f is the velocity of flowing foam, ϕ is the porosity, S_g is the total gas saturation, and r_g and r_c are the lamella generation and coalescence rates, respectively. The generation equation is given as:

$$r_g = k_1 v_w v_g^{1/3} \quad (3.14)$$

The k_1 factor is a constant, and v_w and $v_g^{1/3}$ are the interstitial water and gas velocities, respectively. This equation is given with the assumption that snap-off is the dominant mechanism for lamella generation (Roof 1969, Falls *et al.* 1986).

The equation for coalescence is given as:

$$r_c = k_{-1}\left(P_c\right) v_f n_f \quad (3.15a)$$

$$k_{-1}\left(P_c\right) = k_{-1}^{o} \frac{\left(1 - P_c\right)}{\left(P_c^{*} - P_c\right)} \quad (3.15b)$$

This captures the effect of critical capillary pressure on coalescence by causing the rate of coalescence to approach infinity as the capillary pressure reaches the critical value.

The key output of the population balance is the texture, or lamella density, of the foam which is used to determine the parameters which control the mobility of the foam.

3.2.2.2 Foam Apparent Viscosity

It is assumed by Kovscek (1993) and several other researchers that effective viscosity should scale linearly with bubble density, but this is not supported by experiments. However, Kovscek proposes this expression for the foam apparent viscosity based on the work of Bretherton and Hirasaki:

$$\mu_f = \mu_g + \frac{\alpha n_f}{v_f^c} \quad (3.16)$$

However, pore-network modeling research by Balan (2013) suggests that the relationship between foam apparent viscosity and bubble density is highly nonlinear, although validation of this nonlinear model is currently lacking.

3.2.2.3 Gas Trapping in the Presence of Foam

Most foam modeling studies either: 1) make no attempt to quantify trapped gas in the presence of foam, 2) assume gas trapping is a static process and assign it a constant value, or 3) adopt the correlation below:

$$X_t = X_{t,\max}\left(\frac{\beta n_t}{1+\beta n_t}\right) \quad (3.17)$$

The parameter β is a fitting parameter and $X_{t,\max}$ is the theoretical maximum trapped gas fraction. The trapped gas fraction is used to calculate the flowing gas fraction which modifies the gas relative permeability directly.

Balan (2013) demonstrated through a pore-network upscaling study that gas trapping in the presence of foam is a dynamic process that depends on applied pressure gradient in addition to foam texture. The correlation is given below, and further description and explanation of model assumptions and development are given in the original manuscript.

$$X_{fg} = \frac{1}{2}\left[erfc\left(\frac{x_1 - \ln\left[\left(\nabla P_D \right)_{B'} \right]}{x_2 \sqrt{2}} \right) \right] \quad (3.18)$$

Here X_{fg} is the flowing fraction of gas, $\left(\nabla P_D \right)_{B'}$ is a dimensionless pressure gradient scaled to porous medium properties, and x_1 and x_2 are matching parameters. It should be noted that $\left(\nabla P_D \right)_{B'}$ contains several matching parameters as well, and that the correlation as a whole introduces more complexity than the traditional approach in Eq. 3.17.

3.2.3 Empirical vs. Mechanistic Approach

As in the case of microemulsion modeling the mechanistic approach is rigorous but the number of required parameters that are not readily or routinely obtained introduces empiricism into the model implementation. Furthermore, the current study is focused more on identifying trends and exploring novel interactions rather than developing existing foam models. For that reason, a simplified experimentally-backed model such as that in CMG STARS that focuses on the end-effects of foam, i.e. gas mobility reduction, would be preferable to the mechanistic approach. The empirical model introduced below represents the modified version used for this study.

3.2.4 Empirical Foam Model

To model the foaming process, an inverse mobility reduction factor is directly applied to the gas relative permeability as an aggregate of factors affecting foam stability, with the reduction factor theoretically ranging from 0 (strongest foam allowing no gas flow) to 1 (no foam). The inverse mobility reduction factor takes the form of:

$$RF = \frac{1}{1 + REF * F_{surf} * F_{sal}} \quad (3.19)$$

Here REF represents the mobility reduction factor in the absence of contribution from other factors (i.e. when factors are at their "reference" levels). F_{surf} and F_{sal} refer to contributions from surfactant and salt concentration, respectively.

Surfactant concentration has been shown to increase foam stability when it crosses a critical threshold due to effects on disjoining pressure and micellar structuring, and inversely to decrease foam stability when it falls below that same threshold (Schramm 1994). Therefore, a scaling form of Eq. 3.20 is appropriate for describing the effect of surfactant concentration on foam stability:

$$F_{surf} = \left(\frac{x_{surf}}{f_{surf}} \right)^{a_{surf}} \quad (3.20)$$

Here x_{surf} represents the mole fraction of surfactant in the aqueous phase, f_{surf} represents the critical surfactant mole fraction in the aqueous phase, and a_{surf} is an exponent that determines the degree by which foam stability scales with surfactant concentration.

Based on work done by Srivastava (2010) and Lee *et al.* (2013, 2014), solubilized oil is expected to have a much more significant impact on foam stability for this particular study than bulk, unsolubilized oil. Therefore, our model accounts for the impact of microemulsion phase behavior rather than that of bulk oil. The proxy parameter of salinity (controlling parameter in phase behavior) is employed to capture the detrimental effect of Type III microemulsion.

$$F_{sal} = \left(\frac{x_{salt} - f_{salt,low}}{f_{salt,high} - f_{salt,low}} \right)^{a_{salt}} \quad (3.21)$$

Limits are set according to the minimum salinity $f_{salt,low}$ (maximum contribution to foam mobility reduction) and maximum salinity $f_{salt,high}$ (minimum contribution to foam mobility reduction), corresponding to Winsor Type I and Type III microemulsion regimes, respectively (Eq. 3.21). Both limit parameters as well as the current salinity x_{salt} are given in mole fraction. a_{salt} is an exponent that determines the degree by which foam stability scales with microemulsion phase behavior. Here a_{salt} is taken to be negative in order to describe the inverse relationship between salinity and foam mobility reduction.

The factors taken into consideration are by no means a comprehensive list, but instead are chosen as a minimum set of parameters required to verify trends in mobility reduction without adding unnecessary uncertainty. Gas trapping is modeled as a static process by adjusting the residual gas saturation in the presence of foam. This led to both over- and under-estimation of gas trapping and foam apparent viscosity spatially and temporally but for this work higher priority was placed on the end effect of gas mobility reduction.

3.3 Complete LTG Model Implementation

The complete LTG modeling framework is given in the figure below.

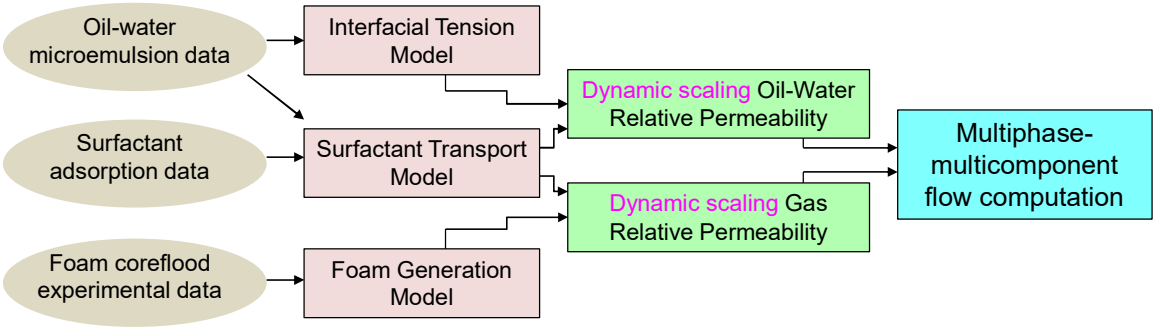

Fig. 3.3: Block diagram showing the workflow of the complete streamlined LTG model.

Simulation models are calibrated based on readily available experimental data and used to calculate oil-water and gas-liquid relative permeability for use in standards multiphase, multicomponent flow calculations.

The model is implemented as an optional subroutine in the CMG GEM compositional simulator which provides an excellent foundation and future extensibility.

Chapter 4: LTG Model Validation: Salinity Gradient Study

4.1 Introduction

Although advances have been made in extending LTG applicability to low permeability, high salinity, and high temperature (Szlendak *et al.* 2012, 2013, 2016, Cottin *et al.* 2012, Nguyen *et al.* 2015, Das *et al.* 2016) conditions, fundamental understanding still needs to be improved to provide a basis for accurate experimental interpretation. One aspect in particular that remains to be explored is the impact of salinity gradient design on LTG flooding performance, and a combined coreflooding and simulation study will provide both LTG model validation and insight into LTG process mechanisms and interactions affecting performance.

4.2 Experimental Description

4.2.1 Objectives

Coreflood objectives are described in Table 4.1, and injection strategies for each flood are presented in Table 4.2. LTG #1 is a base case without gas used as a baseline for LTG performance in the absence of additional foam mobility control. Gas is added at a constant 50% quality (calculated at core temperature and pressure) for both LTG #2 and #3 and slug salinity is reduced from LTG #2 to #3 to demonstrate the sensitivity of oil recovery, mobility control, and microemulsion production to salinity gradient.

Flood ID	Objective	
LTG #1	Base case (no gas injection)	Slug salinity at optimum
LTG #2	Co-injection of gas and chemical solutions	Slug salinity at optimum
LTG #3		Slug salinity at Type I/III boundary

Table 4.1: Coreflood Objectives

Flood ID	Injection rate (liquid +gas)	Gas type	Foam quality	Initial Salinity	Slug size	Slug composition	Drive composition
LTG #1	4 ft./d	None	0%	20,000 ppm	0.3 PV	0.5% C_{20-24} IOS 1% Sec-butanol 19,000 ppm	0.1% C_{20-24}- IOS 6,000 ppm
LTG #2	4 ft./d	N_2	50%	20,000 ppm	0.3 PV	0.5% C_{20-24} IOS 1% Sec-butanol 19,000 ppm	0.1% C_{20-24} IOS 6,000 ppm
LTG #3	4 ft./d	N_2	50%	20,000 ppm	0.3 PV	0.5% C_{20-24} IOS 1% Sec-butanol 16,000 ppm	0.1% C_{20-24} IOS 6,000 ppm

Table 4.2: Coreflood Details

Characteristic properties such as initial and residual oil saturations (S_{oi} , S_{or}) and end point relative permeabilities to oil and water (k_{ro}^{o} , k_{rw}^{o}) are calculated during the coreflood procedure from recorded data such as pressure, injection rate, and mass balance according to effluent collection and are provided in Table 4.3.

Flood ID	k (mD)	Φ (%)	S_{oi} (%)	S_{or} (%)	k_{ro}	k_{rw}
LTG #1	517	25	55	32	0.42	0.11
LTG #2	497	25	55	32	0.46	0.13
LTG #3	522	24	56	33	0.48	0.14

Table 4.3: Rock Properties

4.2.2 Materials

Three 1.5 x 12-inch Berea sandstone cores cut parallel to bedding plane and exhibiting macroscopic permeability ranging from 497 mD to 522 mD were used throughout the experimental series. The cores were dry aged at 120°C for eight to ten days before use. A non-reactive crude oil with a viscosity of 2.9 cP and density of 38 API at 60°C was chosen and a formulation was developed consisting of 0.5 wt. % C_{20-24} internal olefin sulfonate (C_{20-24} IOS) as the primary surfactant and 1.0 wt. % sec-butanol ($C_4H_{10}O$) as a co-solvent to accelerate the equilibration process and prevent the formation of undesired viscous phases. This formulation yielded a high level of oil solubilization, with the Winsor Type III microemulsion window ranging from 17,000 to 21,000 ppm total dissolved solids (TDS) and optimum salinity at 19,000 ppm TDS (Fig. 4.1). The microemulsion phase behavior screening criteria and procedures are in accordance with those described in detail by Flaaten *et al.* (2009).

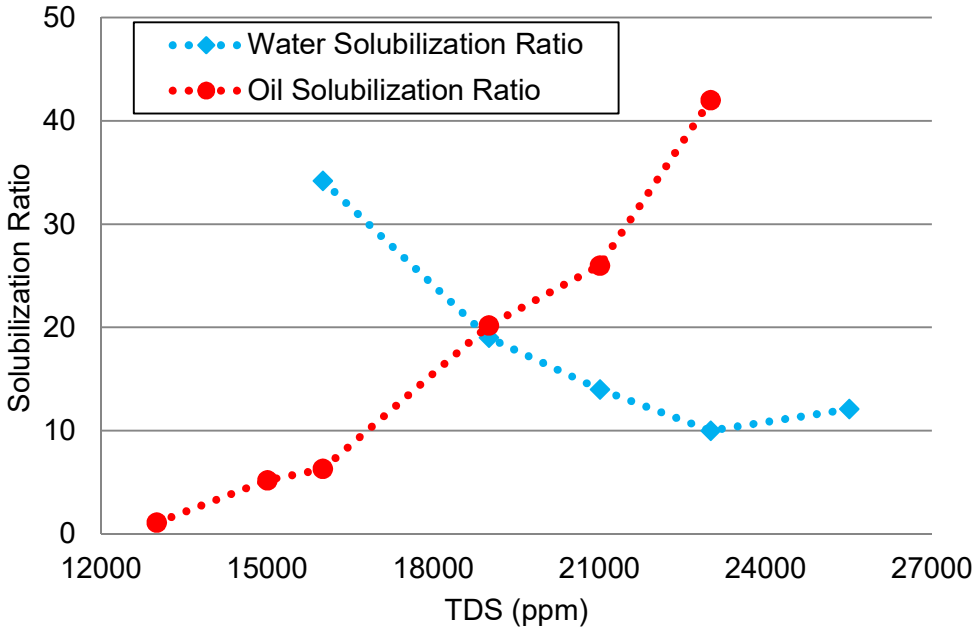

Fig 4.1: Oil and water solubilization ratios vs. TDS.

The synthetic brine and drive solution were composed of only NaCl and deionized water, while the slug contained 1.0 wt. % Na_2CO_3 to reduce adsorption with additional NaCl to reach the desired TDS. Detailed synthetic brine, slug, and drive solution compositions are given in Table 4.2.

4.2.3 Procedure

A schematic of the coreflood apparatus is given below (Fig. 4.2). The core holder is divided in sections three, six, and three inches in length (from bottom to top), respectively, with pressure taps placed along these sections to establish pressure communication. Two back pressure regulators (BPRs) were connected at the outlet of the core to maintain elevated experimental pressure at 300 psi and to reduce the effect of gas expansion on absolute pressure at the core outlet.

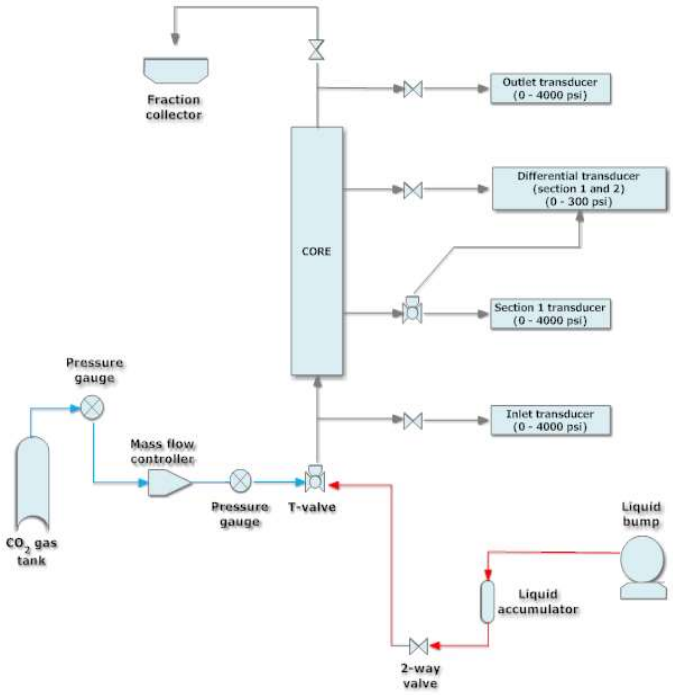

Fig. 4.2: Schematic of coreflood setup.

Liquid injection was controlled by a Quizix QX6000SS pump and gas (N_2) rate (calculated at core temperature and pressure) was regulated by a Brooks SLA5850 mass flow controller that exhibited ±0.5% and ±0.9% error over the injection range, respectively. Gas and liquid were co-injected through a three-way union right before the core inlet without the usage of a foam generator.

The core sample was first wrapped with Teflon and fastened with two end pieces, then covered again with 1.5-inch diameter heatshrink tubing before being inserted into the core holder. Two holes were drilled on pressure taps at four and eight inches along the core holder to create communication with pressure transducers. Valves were fitted to all flow lines and the core holder was placed into an oven at 60°C. The setup was charged with laboratory air to test for leaks and once integrity was verified, the system was placed on vacuum for five to eight

hours. CO_2 was then injected to displace the remaining laboratory air before vacuuming once again to remove CO_2.

Upon completion of vacuuming, several stages of fluid injection were carried out in the following sequence:

1. *Brine Saturation* – Core was saturated completely with synthetic brine. Porosity and pore volume (PV) to liquid were determined during this step through mass balance.
2. *Permeability to brine* – After complete brine saturation, brine was injected at a wide range of flow rates. Pressure drop vs. flow rate relationship was checked for linearity to confirm 100% single phase saturation (i.e. 100% brine and no gas in the system). Permeability to brine was then computed using Darcy's law.
3. *Oil Saturation* – Crude oil was heated up to 60°C and then injected into the core at maximum possible rates while keeping the overall pressure drop below 300 psi. Residual water saturation (S_{orw}), initial oil saturation (S_{oi}), and relative permeability to oil at residual water saturation (k_{rorw}) were calculated within this step using mass balance and Darcy's law.
4. *Water flood* – Oil was displaced by the same brine used in the brine saturation step at 4.0 ft./day in all floods until 100% water cut was obtained in the effluent collection. Relative permeability of brine at residual oil saturation (k_{rwro}) was then calculated. High differential pressure/rate and high permeability cores minimized the impacts from capillary end effects.

5. *Slug injection* – A liquid chemical slug equivalent to 0.3 PV was injected (LTG #1) or co-injected with gas (LTG #2 and #3) at 50% gas fraction to generate foam for mobility control during chemical injection stage.
6. *Drive injection* – A lower surfactant concentration (C_{29-24} IOS only) and lower salinity (6,000 ppm TDS) was co-injected with gas to generate foam for mobility control and improved sweep efficiency. This stage continued until no more microemulsion was obtained in the effluent collection.
7. *Effluent collection and measurement* – Effluent samples were collected at every step (roughly 0.1 PV liquid injection) and used for material balance calculations and salinity analysis. Produced microemulsion was heated at 90°C to collect pure oil for recovery calculations.

4.2.4 Simulation Set-Up

Each case was set up on a 1x1x32 grid (oriented vertically) and incorporates experimentally measured core properties including porosity and permeability. Low capillary number limit relative permeability data were obtained by history matching waterflood data for each coreflood. LTG #1 (no gas injection) was used as a base case for microemulsion phase behavior calibration, with LTG #2 and #3 using the same calibrated parameters. This allowed for a minimum set of parameters constrained by uncertainty and physical feasibility to be varied in any given run in order to obtain unique explanations of coreflood results.

The main simulation parameters for the LTG cases (#2 and #3) were the intermediate capillary number oil-water relative permeability curves, gas-liquid relative permeability curves, CMC (proxy for adsorption), and longitudinal

dispersivity coefficient, all of which are rock-dependent and should vary from case to case. It should be noted that the classical CMC refers to the surfactant concentration above which interfacial tension is no longer reduced and micelle formation is favored. However, in simulation it is useful to implement CMC as a lower limit to describe the minimum amount of surfactant that may practically be injected due to adsorption constraints.

The goal of the simulation component was to obtain physical explanations of the results observed during the experiments, keeping in mind the limitations of both the experimental data and the LTG model itself. Discrepancies between experiments and simulation may therefore be due to either or both of these limitations and will be examined closely in the Results and Discussion section below.

4.3 Results and Discussion

4.3.1 Base Case vs. Mobility Control

LTG #1 (no gas injection, slug injection at optimum salinity) is compared with LTG #2 (gas-chemical co-injection, slug injection at optimum salinity) to demonstrate the effect of mobility control on LTG performance in terms of oil recovery, pressure drop, and salinity profiles during chemical injection.

Figure 4.3 shows an improvement in oil recovery during chemical injection from 45% to 71% residual oil in place (ROIP) from LTG #1 to LTG #2. There was significant increase in residual oil recovery, a larger oil bank, a higher oil cut at the early stage of production (0 to 0.6 PV), and a faster production response in LTG #2, corresponding to mobility reduction of injected fluids that results in more favorable mobility ratios and better displacement efficiency.

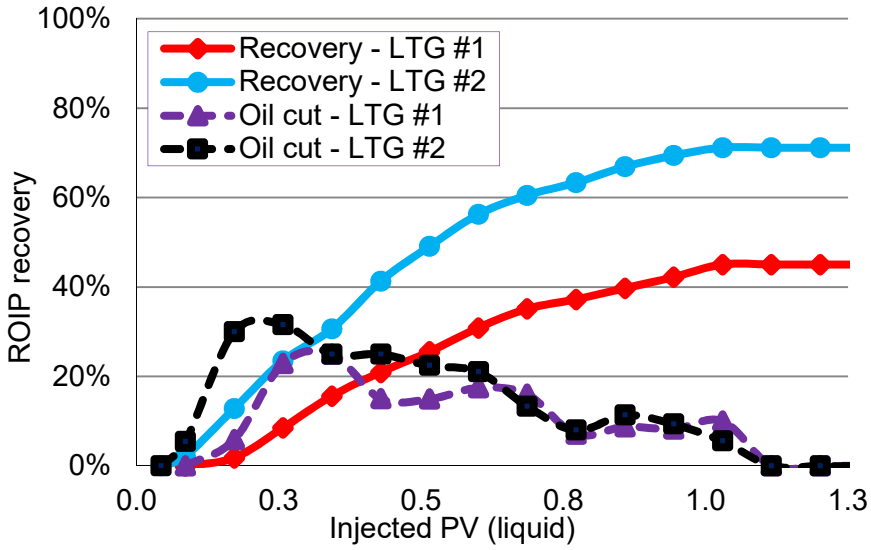

Fig 4.3: Oil recovery and oil cut for LTG #1 and LTG #2.

Conversely, a much more gradual production profile was obtained from LTG #1, indicating elongation of the oil bank due to the lack of mobility control. Notice that LTG #2 also demonstrated an elongated oil bank despite the higher oil recovery and reached ultimate oil recovery around the same time as LTG #1 in terms of liquid PV injected.

Although the oil recovery and oil cut shown in Fig. 4.3 indicate an oil bank, the pressure data do not show an increase in pressure associated with the buildup of an oil bank (Fig. 4.4). This may be due to the fact that oil had a higher endpoint relative permeability than water so that the oil bank buildup resulted in the early time decrease in pressure observed.

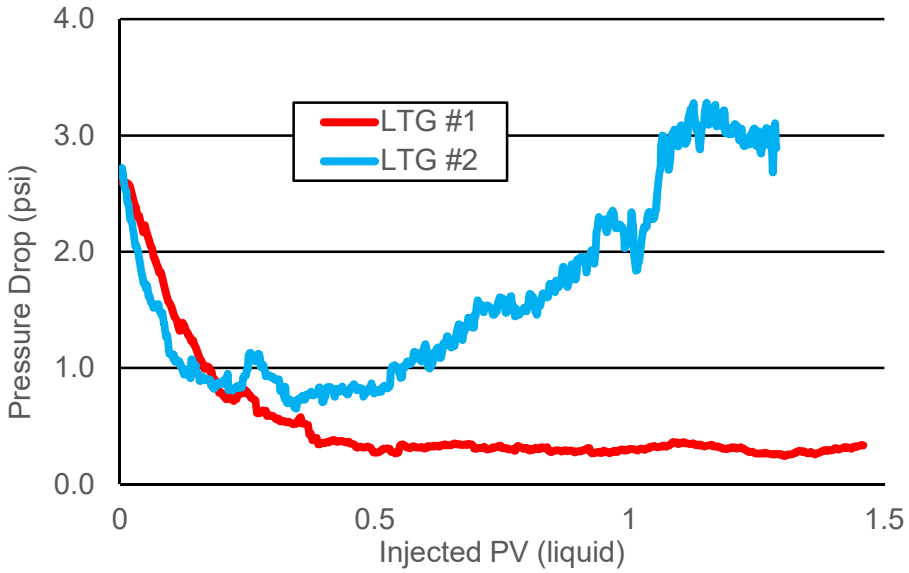

Fig. 4.4: Pressure drop for LTG #1 and LTG #2.

An increase in pressure drop at late-stage drive injection in LTG #2 compared to the gradual decline in LTG #1 indicates foam presence during chemical injection. This trend is characteristic and indicative of foam generation and propagation in the LTG process (Srivastava *et al.* 2010, Srivastava 2010) and may be because the lower salinity environment of the drive (and greater prevalence of Winsor Type I compared to Winsor Type III microemulsion) was more conducive to stable foam.

The greater degree of mobility control achieved may also be demonstrated through the effluent salinity profile (Fig. 4.5), with a sharper profile indicating greater mobility control. The collected effluent samples contained both Na_2CO_3 and NaCl, although a compositional analysis was not performed to determine separate conductivity contributions. However, the collection and measurement procedure were consistent throughout the entire study and support the validity of the observed and compared trends.

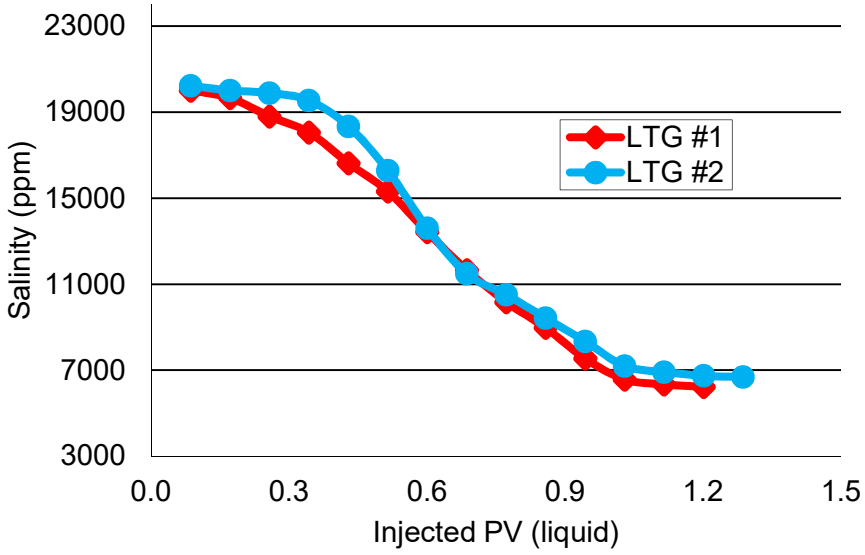

Fig. 4.5: Effluent salinity for LTG #1 and LTG #2

The effluent salinity profile of LTG #1 shows the typical result of dispersive mixing, as the original stepwise transitions in salinity were severely smoothed out. In LTG #2, the formation salinity is produced for the first 0.3 PV followed by a sharp decrease as the slug and drive were injected up until around 0.7 PV, evidence of reduced dispersive mixing. After 0.7 PV, the profile became anomalously less sharp due to measurement error. This error was probably caused by combining effluent samples to obtain adequate sample size for more accurate measurement of produced oil and effluent water conductivity.

The LTG model was able to explain the results of LTG #1 and LTG #2 well (matches shown in Figs. 4.6 and 4.7), demonstrating clearly the improvement in oil recovery and associated pressure drop profile due to foam mobility control.

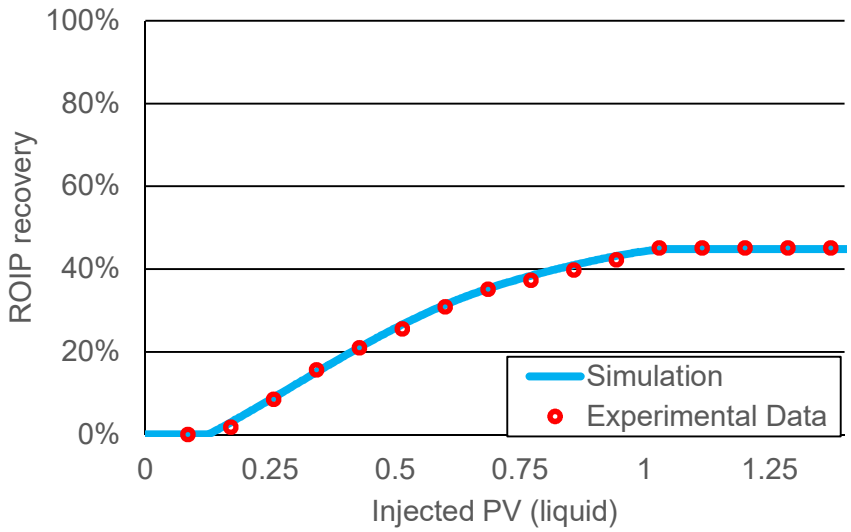

(a)

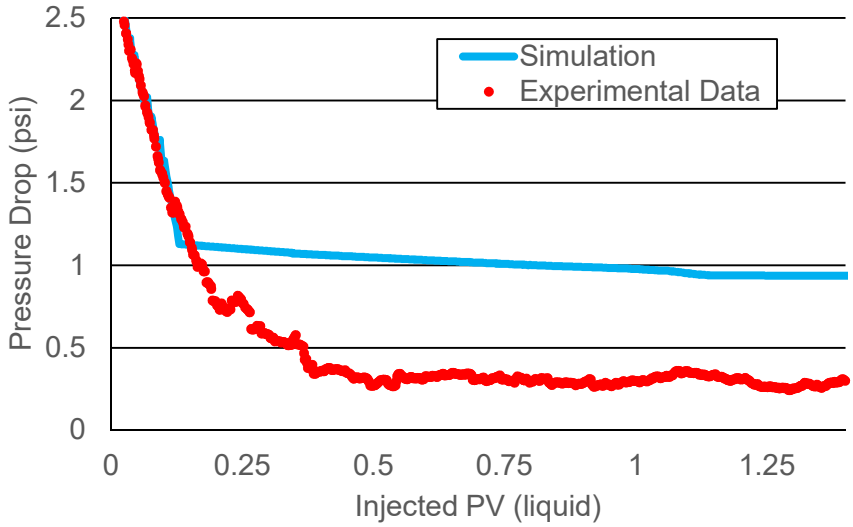

(b)

Fig. 4.6: LTG #1 simulation results for (a) oil recovery and (b) pressure drop.

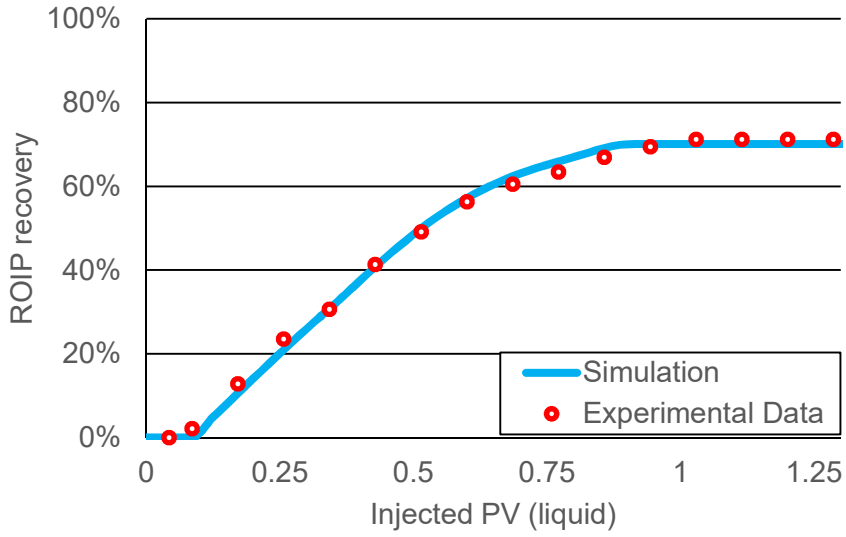

(a)

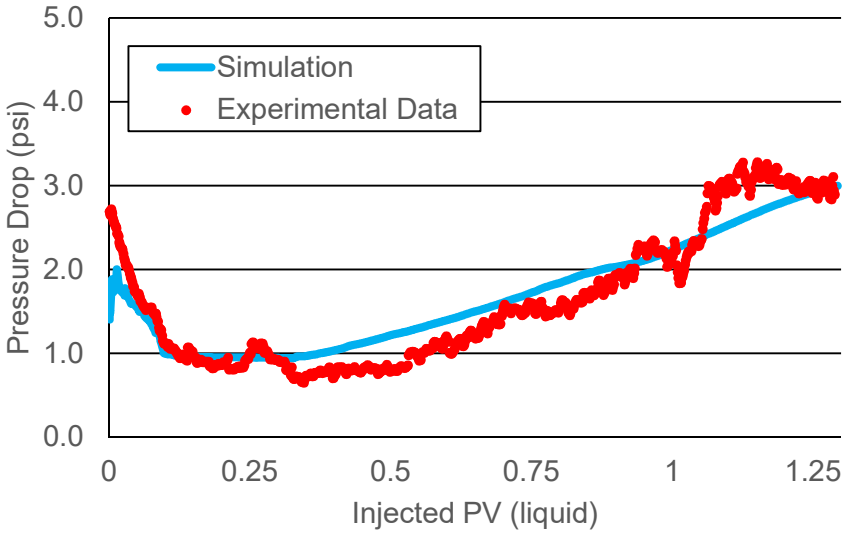

(b)

Fig. 4.7: LTG #2 simulation results for (a) oil recovery and (b) pressure drop.

The simulation results also confirmed the analysis regarding the degree of dispersive mixing, with a reduction in longitudinal dispersivity coefficient from LTG #1 to #2 (Table 4.4).

Property	LTG #1	LTG #2	LTG #3
REF	-	5.5	6.2
$f_{salt,low}$ (mol. frac. NaCl)	-	0.0011	0.0015
$f_{salt,high}$ (mol. frac. NaCl)	-	0.0121	0.0095
a_{salt}	-	-2.030	-1.306
f_{surf} (mol. frac. surf.)	-	2.303×10^{-5}	2.021×10^{-5}
a_{surf}	-	0.27	0.76
CMC (mol. surf. /kg water)	3.03×10^{-4}	6.51×10^{-5}	3.31×10^{-5}
Dispersion (m)	0.374	0.085	0.017
Intermediate Cap. No. (Log)	-2.86	-4.09	-4.87
$n_{o,2}$	1.00	1.00	1.36
$n_{w,2}$	2.68	1.98	2.46
$S_{orw,2}$	0.192	0.088	0.156
$S_{wro,2}$	0.226	0.378	0.420
$k_{rorw,2}$	0.806	1.000	0.998
$k_{rwro,2}$	0.199	0.285	0.166
n_{og}	N/A	1.30	3.87
n_g	N/A	1.47	2.53
S_{gr}	N/A	0.100	0.129

Table 4.4: Simulation Parameters

When dispersive mixing is reduced in a surfactant EOR process, the chemical profiles for salinity and surfactant concentration are sharpened, resulting

in increased process efficiency and effectiveness. In addition the CMC, here a proxy for surfactant adsorption, decreased from LTG #1 to #2. Reducing the mixing between synthetic brine, slug, and drive salinities resulted in a quicker transition from a high to low salinity environment which has been shown to reduce adsorption of anionic surfactants (Noll and Gall 1991, Azam *et al.* 2013).

By comparing the exponents of the power law relations obtained through matching (Table 4.4) to describe the relative importance of surfactant concentration and microemulsion phase behavior on foam stability, it was found that foam stability is much more sensitive to microemulsion phase behavior than to surfactant concentration for the given system as the net effect of decreased salinity and surfactant concentration was overwhelmingly positive in terms of foam stability.

4.3.2 Effect of Slug Salinity Reduction (Reduced Slug Salinity Design)

Slug salinity was reduced from optimum salinity to the Winsor Type I range in LTG #3 while holding other properties constant (Table 4.2) to study the effects of varying salinity gradient design on the LTG process.

Comparison of oil recovery in LTG #2 and #2 (Fig. 4.8) shows improvement upon reduction of slug injection salinity, with an ultimate oil recovery of 82% at roughly 1.1 PV liquid injection for LTG #3.

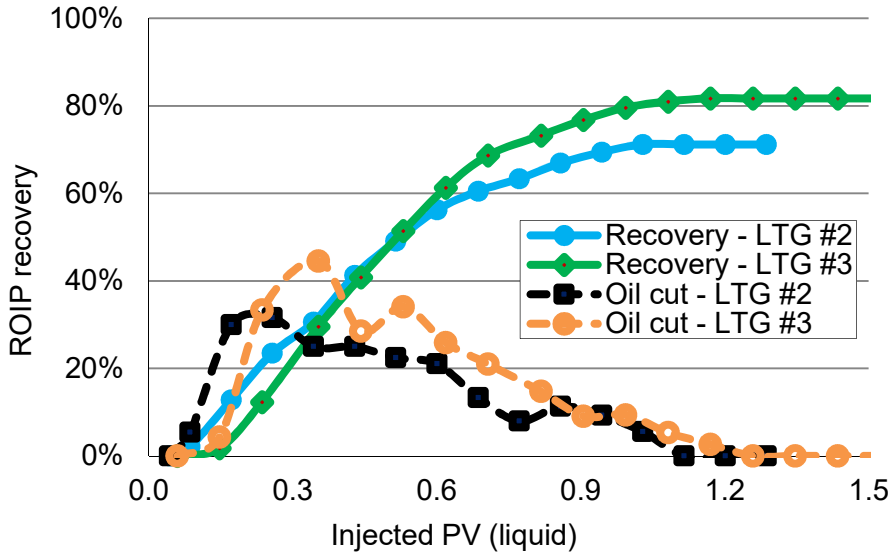

Fig. 4.8: Oil recovery and oil cut for LTG #2 and LTG #3.

LTG #2 exhibited earlier production than LTG #3 in the first 0.35 injected PV but then continued with more gradual recovery, ultimately achieving only 71% oil recovery compared to 82% for LTG #3. LTG #2 had a more gradual transition to the drive salinity than LTG #3 (Table 4.2) and thus should have had more Winsor Type III behavior. While this facilitated ultralow oil-water IFT and the mobilization of residual oil, it may also have been detrimental to foam stability. As a result, while LTG #2 had the potential to mobilize more oil than LTG #3, insufficient mobility control led to inefficient displacement of the oil bank and the more gradual recovery slope after 0.35 PV.

As the environment created by mixing of the slug salinity with synthetic brine salinity deviated from the Winsor Type III region in LTG #3, foam destabilization was reduced while ensuring that the salinity gradient still passed through the region for ultra-low oil-water IFT. This resulted in more effective mobility control during

slug injection and thus higher and faster oil production due to favorable and stable propagation of the mobilized and reconnected oil.

Decreasing slug salinity reduced the overall efficiency of the surfactant slug by limiting the amount of Winsor Type III behavior but also increased foam stability, as evidenced by the increase in pressure drop during slug injection from LTG #2 to #3 (Fig. 4.9).

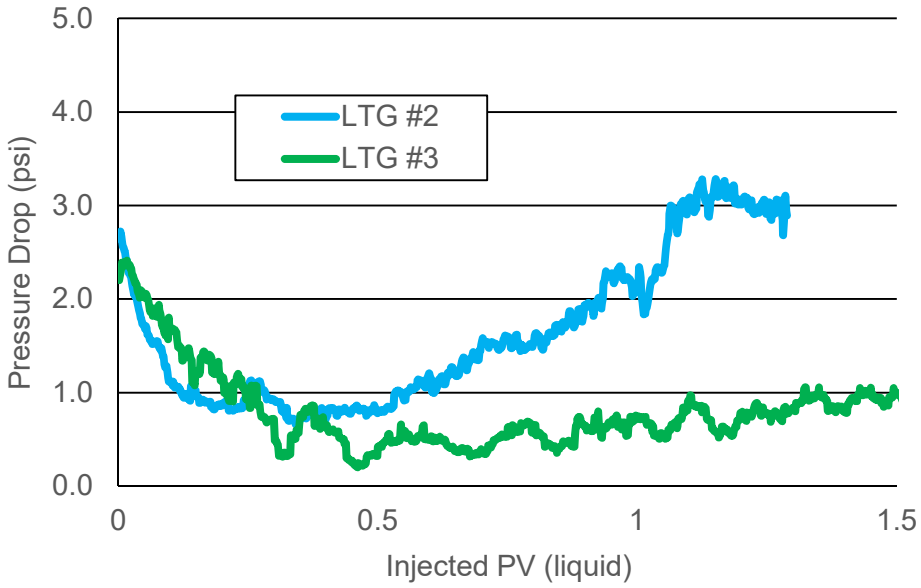

Fig. 4.9: Pressure drop for LTG #2 and LTG #3.

However, the pressure drop in LTG #2 increased and exceeded that of LTG #3 at the end of drive injection due to higher saturation of immobile oil after chemical injection (lower final oil recovery compared to LTG #3), which consequently resulted in lower gaseous and aqueous relative permeability compared to LTG #3.

The pressure drop behavior during the first 0.1 PV of liquid injection for LTG #2 and #3 was due to the combination of gas influx and foam destruction. Because

the co-injection point was separated from the core by a finite distance (Fig 4.2), foam was formed in the injection line before reaching the inlet. The capillary contrast from the injection line to the core resulted in a dramatic collapse of the foam from the line, resulting in the sharp pressure decrease during the first 0.1 PV of liquid injection. The starting points of the simulation pressure drops agree with the post-waterflood steady state pressure drop data observed during the experiments.

The salinity gradient comparison in Fig. 4.10 showed that dispersive mixing decreased due to the increase in foam mobility control and resulted in a sharper profile for LTG #3 compared to LTG #2.

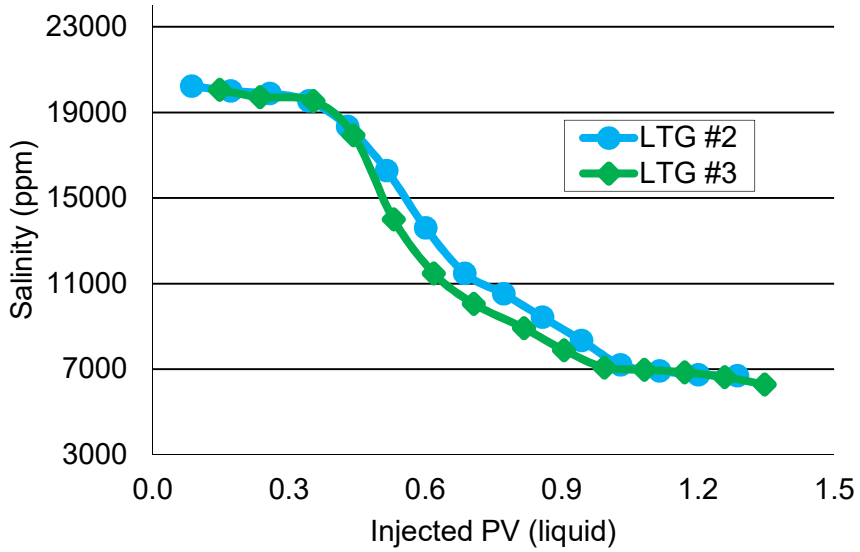

Fig. 4.10: Effluent Salinity for LTG #2 and LTG #3.

The simulation study (Fig. 4.11) revealed a further reduction in dispersion (Table 4.4), which when combined with the lower injection salinity led to a quicker transition to Winsor Type I salinity and a lower final salinity.

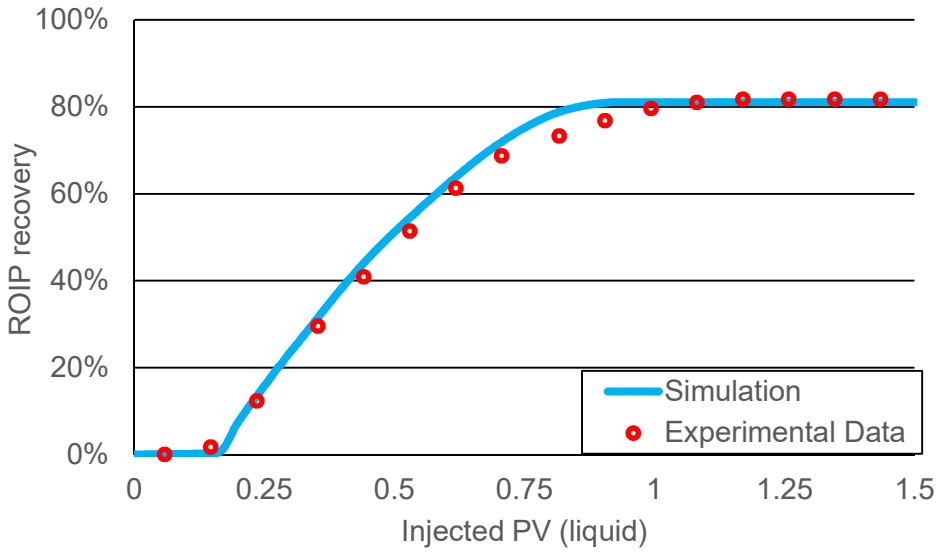

(a)

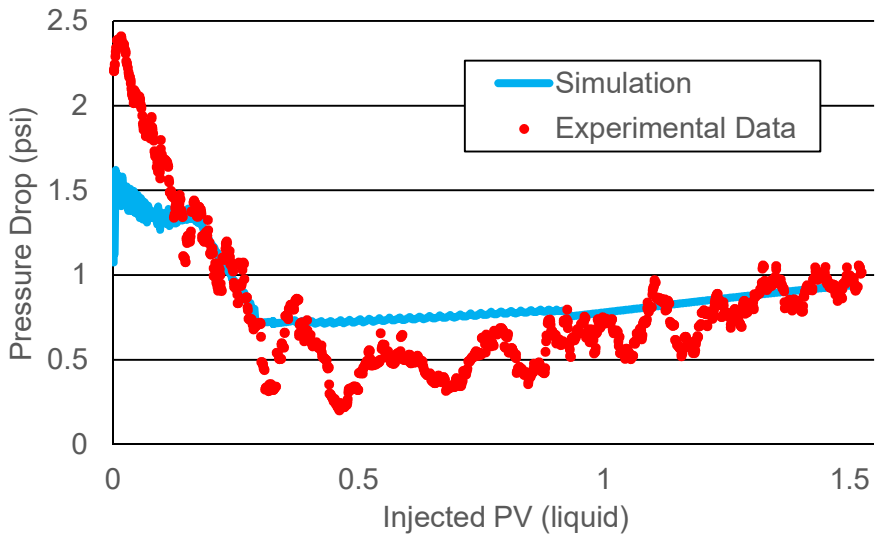

(b)

Fig. 4.11: LTG #3 simulation results for (a) oil recovery and (b) pressure drop.

This improved the foam stability (increase in mobility reduction factor from LTG #2 to LTG #3 of 15.2 to 19.7 and an increase in gas trapping through an increase in gas residual saturation from 0.100 to 0.129) and reduced adsorption due to the lower average salinity (CMC reduction from LTG #2 to LTG #3), which were able to compensate for the reduced duration of ultra-low oil-water IFT conditions.

Reducing salinity also increased pure oil production and decreased emulsified oil or microemulsion production over the chemical injection stages (Table 4.5). This increase in pure vs. emulsified oil production was due to a combination of the reduced amount of Winsor Type III microemulsion due to lower salinity environments and the increased foam strength with less Winsor Type III microemulsion which provided improved liquid mobility control and effective oil displacement. The increased foam strength also reduced dispersive mixing to yield a quicker transition from a Winsor Type III environment to a Winsor Type I environment, demonstrating both forward and inverse interactions.

Property	LTG #1	LTG #2	LTG #3
Microemulsion production (v/v %)	35	56	40
Pure Oil Production (% ROIP)	21	30	52
Oil from Microemulsion (% ROIP)	24	41	30
Residual Oil Recovery (% ROIP)	45	71	82
Recovery of OOIP (% OOIP)	37.4	45.7	50.1

Table 4.5: Pure and Emulsified Oil Recovery

4.4 KEY FINDINGS

1. The experimental results demonstrated that the traditional optimal salinity gradient design for surfactant flooding guaranteeing more Winsor Type III behavior and ultra-low oil-water IFT could be detrimental to foam stability and leads to inefficient displacement of mobilized oil. This may be due to microemulsion phase behavior, which changes significantly with salinity.
2. Reducing the slug salinity leads to more stable foam, improved surfactant transport and reduced adsorption, better mobility control and reduced dispersive mixing, and higher and faster ultimate oil recovery despite reducing the amount of Winsor Type III behavior. Pure oil vs. microemulsion production ratio as well as oil recovery may be improved by lowering slug salinity (approximately 57% increase and 15% increase, respectively).
3. Designing an LTG flooding salinity gradient requires balancing between reducing oil-water IFT for oil mobilization and achieving adequate mobility control for oil displacement.
4. Simulation study revealed the significant contribution of gas trapping to foam mobility control, with up to 0.129 PV of trapped gas and an increase in gas trapping with the increase in foam strength from LTG #2 to LTG #3.

Chapter 5: Further Investigation of Microemulsion-Foam Interactions

5.1 Introduction

During chemical injection in the LTG flooding process, different portions of the reservoir are subjected to a range of microemulsion phase behavior as injection salinity (electrolyte concentration) is altered. As salinity is increased for a given system of surfactant, oil, and brine the phase behavior will change from Winsor Type I to Winsor Type III to Winsor Type II, which correspond to an aqueous microemulsion phase with solubilized oil (within surfactant micelles) in equilibrium with excess oil, a bicontinuous middle phase microemulsion with solubilized oil and water in equilibrium with excess oil and excess water, and an oleic microemulsion phase with solubilized water (within inverted surfactant micelles) in equilibrium with excess water, respectively. The work done in the previous chapter on the impact of changing salinity environments on LTG performance indicates that varying microemulsion phase behavior has a strong impact on foam stability.

Theory and experimental work indicate that oil-swollen micelles may affect micellar structuring and decrease foam stability compared to oil-free micelles due to reduced intramicellar repulsion. It is postulated that the interaction of microemulsions and foams may be explained by the micelles, which are dispersed within an external phase to comprise microemulsions. The current work is constrained to Winsor Type I microemulsions because their influence on foam stability may be readily compared to the oil-free foam stability case due to Winsor Type I microemulsion still being a predominantly aqueous phase with surfactant micelles (albeit oil-swollen) that provide structuring when confined to an aqueous

film. Increasing salinity within the Winsor Type I region will produce a range of microemulsions which differ in readily quantifiable properties such as oil concentration and oil-swollen micelle diameter.

5.2 Experimental Description

5.2.1 Objectives

Foam stability to various microemulsions was studied first at the bulk scale in order to verify previously observed trends and then at the confined porous medium scale in order to determine the scaling of microemulsion-foam interactions. If the trends proved similar, then it would indicate that a bulk foam stability test would be a reasonable routine screening procedure for microemulsion-foam interactions in an LTG process. Furthermore, the static nature of the confined tests served to shed light on the evolution of far-field trapped foam texture.

5.2.2 Materials and Phase Behavior

Several surfactant-crude oil systems were screened for microemulsion and foam generation potential and a wide Winsor Type I microemulsion range with significant oil solubilization. The selected system consisted of A 1:1 ratio of C_{15-18} internal olefin sulfonate (IOS) and C_{16-17}-7PO alcohol alkoxy sulfate for the anionic surfactant blend and a light (37.1 API gravity at 35°C), low viscosity (3.1 cP at 35°C) crude oil.

An aqueous stability test was conducted to identify the critical salinity (in wt. % NaCl) above which the surfactant blend precipitated. After the critical salinity was determined, 350.0 µL of 4.0 wt. % surfactant stock, 400.0 µL of crude oil, and varying amounts of 14.0 wt. % NaCl and deionized water (resulting in 2.8 mL total

aqueous solution with 0.5 wt. % surfactant concentration) were dispensed into Fisherbrand 5.0 mL borosilicate serological pipettes to perform a salinity scan for phase behavior. The pipettes were heat-sealed and allowed to equilibrate in a convection oven at 35°C for seven days and subjected to inversion six times per day to promote mixing. Phase behavior and aqueous stability results indicated Winsor Type I microemulsion phase behavior (Fig. 5.1) and aqueous stability up to 9.0 wt. % NaCl.

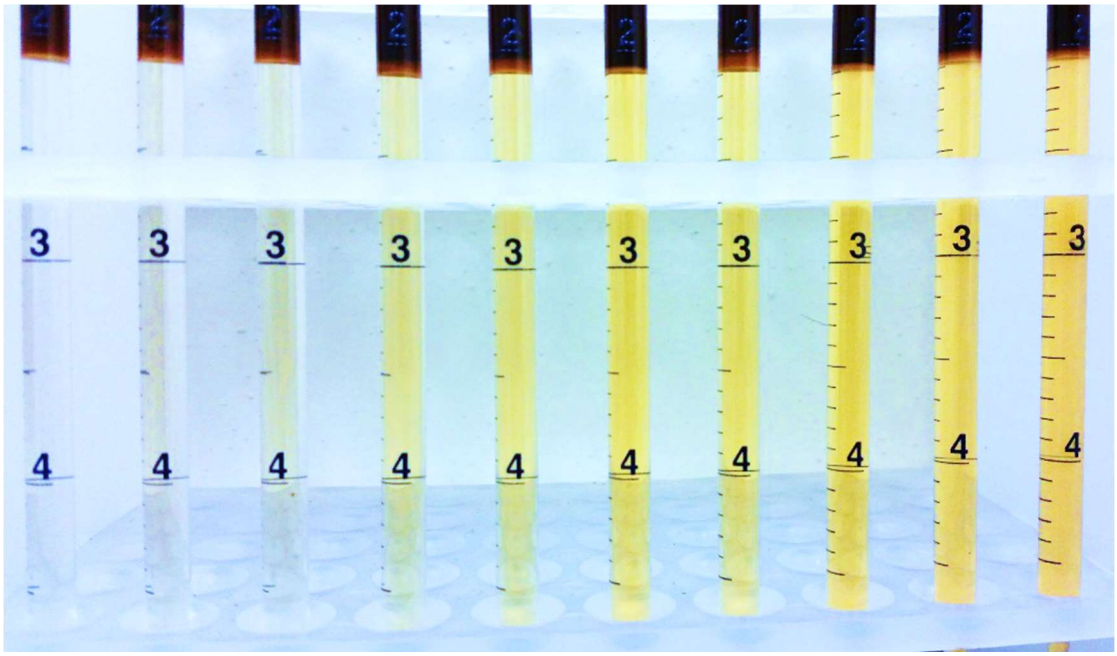

Fig. 5.1: Phase behavior results from 2.0 wt. % NaCl to 6.5 wt. % NaCl demonstrating transition with salinity.

Seven samples were chosen within the Winsor Type I range to represent varying degrees of oil solubilization. The maximum salinity chosen was 7.0 wt. % NaCl in order to avoid the transition zone between Winsor Type I and Type III microemulsions. Sample properties are listed in Table 5.1.

Sample	Salinity (wt.% NaCl)	Oil Concentration (v/v %)	Oil-Swollen Micelle Diameter (nm)	Viscosity at 15 s^{-1} and 35 °C (cP)
1	2.0	0.93	9.30	0.86
2	3.5	1.09	11.86	0.96
3	4.5	1.57	13.80	0.95
4	5.5	1.93	16.63	0.96
5	6.0	2.41	18.26	0.98
6	6.5	2.89	20.65	0.91
7	7.0	3.92	27.08	0.91

Table 5.1: Summary of Sample Properties

The same procedure was followed to produce larger quantity samples, substituting Fisherbrand borosilicate test tubes for pipettes and removing excess oil via suction before extracting the equilibrated microemulsion phase into secondary test tubes. Microemulsion extraction occurred from the bottom of the original test tubes and ceased when approximately 3.0 mL of sample remained to avoid taking any sample from near the original microemulsion-excess oil interface. Diluted samples for 2.0, 4.5, and 6.0 wt. % salinity were also produced at 50.0%, 25.0%, and 12.5% original oil-swollen micelle concentration by mixing undiluted samples with equivalent salinity NaCl solutions in order to control micelle size while varying micelle concentration.

5.2.3 Microemulsion Characterization

The oil-swollen micelles in each microemulsion sample were characterized according to particle size and concentration. Size measurements were made using a Malvern Nanosizer ZS, a dynamic light scattering (DLS) machine, and are shown in Fig. 5.2.

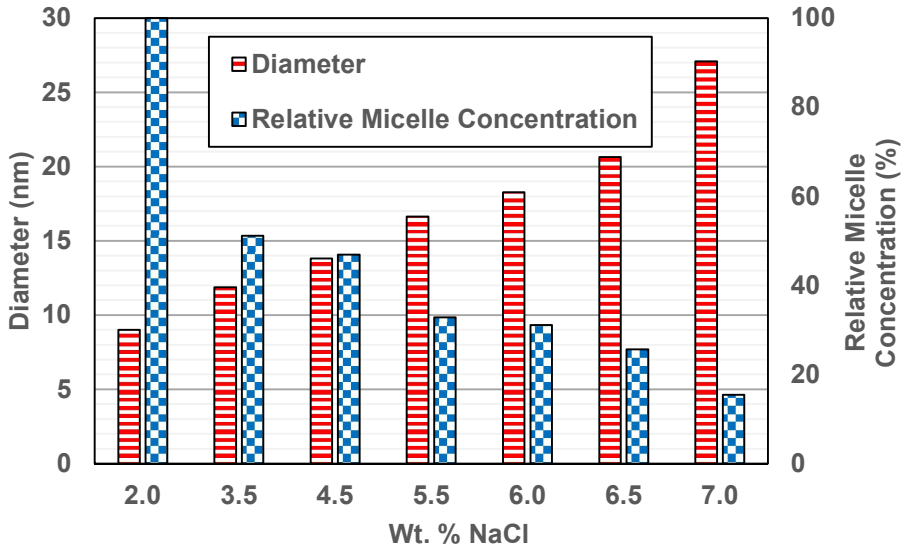

Fig. 5.2: Diameter and relative micelle concentration for all samples.

These measurements agree with theoretical calculations and previous measurements of droplet size for microemulsion systems (Huh 1979). Micelle size is in the range of 9.0-28.0 nm and increases with increasing salinity within the Winsor Type I region with a trend that resembles the oil solubilization ratio. This is expected because the oil solubilization ratio and droplet size are linked by the propensity of surfactant to adsorb at oil-water interfaces, which is controlled by the ion concentration in the aqueous phase.

In the phase behavior scan, upward movement of the oil-water interface with increasing salinity corresponded to increasing oil solubilization. Measurement of the amount of oil remaining allowed for calculation of oil volume fraction in the aqueous phase. Table 5.1 includes the oil concentration in the aqueous phase for each sample.

Oil volume fraction in the aqueous phase is only an intermediate step, since it is determined by the size and concentration of oil-swollen micelles. Therefore, an approach was taken to normalize the solubilized oil to the volume of oil-swollen micelles from DLS measurement, assuming approximate sphericity and relative monodispersity (DLS dispersity for all samples was less than 20.0%, indicating monodispersity), before normalizing to microemulsion volume (which itself increased with increase in oil solubilization). Finally, the results for samples 1-7 (Table 5.1) were divided by the result for sample 1, giving a relative indication of oil-swollen micelle concentration for each sample.

The results in Fig. 5.2 demonstrate an increasing micellar aggregation number with increasing neutral electrolyte addition, as decreased repulsion between hydrophilic head groups allowed for closer packing due to compression of the electrical double layer, larger micelles, and greater oil solubilization per micelle (Rosen and Kunjappu 2012). This factor outweighed the simultaneous decrease in CMC with increasing neutral electrolyte addition to result in net decrease of oil-swollen micelles.

5.2.4 Surface Tension and Critical Micelle Concentration (CMC) Measurements

In order to determine whether microemulsion-foam interactions were due solely to the action of oil-swollen micelles within liquid lamellae or involve

contribution from interactions with the air-water interface, several series of surface tension measurements were performed.

The measurement system consisted of a ramé-hart F4 Series camera focused on a flat Teflon surface and placed opposite a 150w fiber optic illuminator. Measurements were made in the sessile drop mode via ramé-hart DropImage Advanced software, which captured the curvature of the drop and calculated surface tension via Young-Laplace methods.

A CMC measurement was conducted first with varying concentrations of surfactant in deionized water to gauge the maximum reduction in surface tension achievable with surfactant only. Afterwards, measurements were performed for surface tension of surfactant solutions well above CMC (0.5 wt. % corresponding to the concentration in undiluted microemulsion samples) with varying salinities corresponding to the seven microemulsion samples (no oil was added) in order to gauge the base effect of increasing neutral electrolyte concentration. Finally, measurements were performed for surface tension of the seven microemulsion samples to determine the presence or absence of free surfactant monomers in equilibrium with oil-swollen micelles.

5.2.5 Bulk Dynamic Foam Stability Setup

Dynamic foam stability was measured at the bulk scale in order to obtain a baseline for microemulsion-foam interactions for comparison to microfluidic scale interactions. The setup consisted of a 1000 mL Fisherbrand KiMax burette fixed vertically on a ring stand with 1/8-inch stainless steel tubing inserted in the center from the top onto a ring stand and placed the setup inside an oven at 35°C.

For each microemulsion sample, 3.0 mL of the sample was dispensed into the burette and CO_2 was bubbled into the sample from the base of the burette at a rate of 160.0 standard cubic centimeters per minute (SCCM). The experiment continued until the foam coalescence rate due to capillary suction and gravity drainage was equivalent to the foam generation rate due to bubbling CO_2. The equilibrium height was recorded as a measure of the samples' dynamic foam stability before the burette was rinsed thoroughly with deionized water and dried with high pressure laboratory air.

This Bikerman-style experiment had the advantage of eliminating variance in initial states between samples while also providing monodisperse generation of new foam bubbles. Since these experiments were performed with pre-equilibrated Winsor Type I microemulsions free of excess or bulk oil, any change in foam stability was attributed to the presence of oil-swollen micelles.

5.2.6 Microfluidic Static Foam Stability Setup

To extend the bulk foam study findings to porous media applications, an experimental setup was developed to examine foam stability in a porous media microfluidic model. A diagram of the setup is shown in Fig. 5.3.

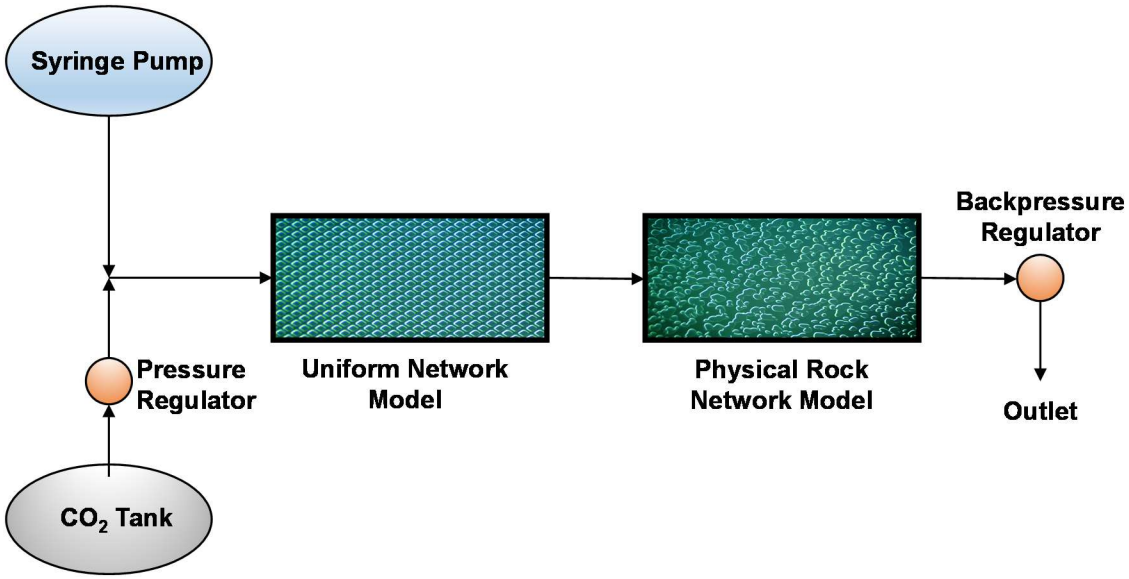

Fig. 5.3: Block Diagram representation of microfluidic static foam stability setup.

CO_2 was routed from a tank maintained at 800 psi and joined to a chemical solution-bearing Hamilton Gas Tight Syringe seated in a Chemyx Fusion Syringe Pump via a three-way union, analogous to the co-injection setup used for core flooding. CO_2 was maintained at a constant upstream pressure of 25 psi and chemical solution injection rate was set at 5 µL/min. Liquid and gas were co-injected into a Micronit borosilicate glass uniform microfluidic network (45.0 x 15.0 mm chip size, 50.0 µm channel width, 20.0 µm channel depth) to promote mixing and monodisperse bubble generation before entering into a Micronit borosilicate glass microfluidic network based on a physical rock (45.0 x 15.0 mm chip size, 50 µm channel width, 20.0 µm channel depth). A 20-psi backpressure regulator was connected to the outlet of the chip in order to avoid larger gas pressure fluctuations associated with a lower pressure range. Gas injection was thus maintained at a

constant 2.5 psi pressure drop across the chip. Pressure drop along the lines amounted to roughly 2.5 psi.

Each microemulsion sample was co-injected with CO_2 to generate and propagate foam in the physical rock network chip before shutting in the system. The relatively high rate of injection led to a uniform initial texture (number of foam bubbles per unit area) for all samples since generation dominated coalescence. Decay was observed and recorded for 30 minutes via an AmScope MU300 Microscope Digital Camera connected to a laptop computer. After 30 minutes, the chip was flushed extensively with deionized water to remove surfactant followed by dichloromethane to remove any oil left behind by microemulsions and 40 minutes of CO_2 injection to ensure complete removal of dichloromethane before beginning the next experiment. Image analysis was performed using ImageJ and initial and final texture were recorded for each sample.

5.3 Results and Discussion

5.3.1 Surface Tension Measurements

Once surfactant concentration in the aqueous phase has increased past CMC, minimal change is observed in surface tension because surfactant has already reached maximum adsorption at the interface (Rosen and Kunjappu 2012). Additional surfactant leads to the formation of micelles that are in equilibrium with surfactant monomers (Mysels and Otter 1961, 1961, Shah *et al.* 1996). These surfactant monomers ought to be present by definition at a concentration below CMC, else micelle formation is favored over independent monomers.

Winsor Type I microemulsions are comprised of oil-swollen surfactant micelles suspended in aqueous solution. These oil-swollen micelles only depress

CMC slightly and are not found to adsorb at the air-water interface at equilibrium (Rosen and Kunjappu 2012). However, there is no previous work which indicates whether surfactant monomers exist in equilibrium with oil-swollen micelles.

Therefore, surface tension measurements were approached with an expectation of one of two outcomes:

a) Surface tension of microemulsions is higher than that of equivalent oil-free samples of varying salinity, indicating reduced availability of tendency of surfactant monomers to adsorb at the interface.
b) Surface tension of microemulsions is equal to that of equivalent oil-free sample of varying salinity, indicating equivalent availability or tendency of surfactant monomers to adsorb at the interface.

Testing of the oil- and NaCl-free surfactant solutions indicated a CMC of 0.046 wt. % and minimum surface tension of 31.79 dynes/cm. Addition of various amounts of NaCl at 0.5 wt. % concentration resulted in a small surface tension reduction to an average of 28.36 dynes/cm (Fig. 5.4), which was nearly constant across all samples (0.54 dynes/cm standard deviation).

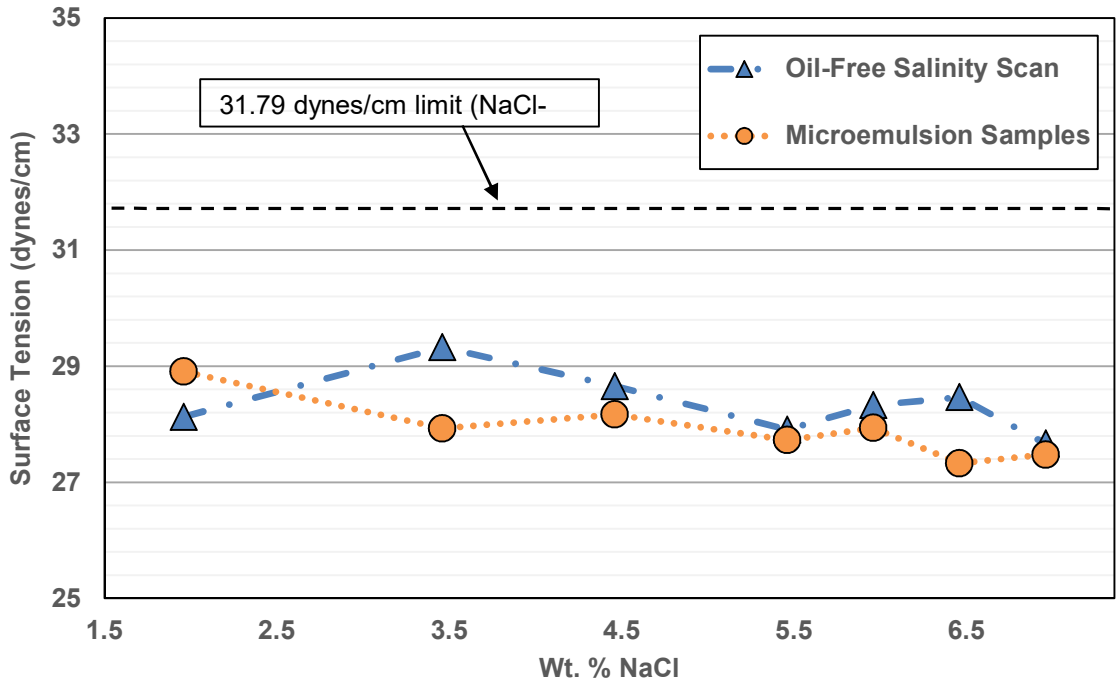

Fig. 5.4: Surface tension vs. salinity for oil-free and microemulsion samples.

Increased neutral electrolyte concentration in a surfactant solution leads to more efficient monomer adsorption at the air-liquid interface and lower surface tension (Ross and Bramfitt 1957), although within this range near-maximum adsorption at the air-liquid interface has already been achieved.

The same increase in neutral electrolyte concentration also leads to larger micelles, which can solubilize more oil. However, these were not found to have any additional effect on the air-liquid interface as the surface tension remained at an average of 27.93 dynes/cm (0.52 dynes/cm standard deviation) (Fig. 5.4). Based on these measurements and observations, it can be concluded that surfactant monomers are present and in equilibrium with oil-swollen micelles, which is in line with the second expected outcome.

Therefore, there is confidence in the analysis of proceeding experimental results in terms of intra-film micellar interactions rather than interfacial phenomena due to reduced surfactant monomer availability in the presence of oil-swollen micelles.

5.3.2 Bulk Foam Stability Testing

The results of the bulk foam stability test (Fig. 5.5) for the undiluted samples indicated a strong impact of microemulsion phase behavior on foam stability. The results were normalized to the control case of an oil-free sample whose stability was shown to be independent of salinity.

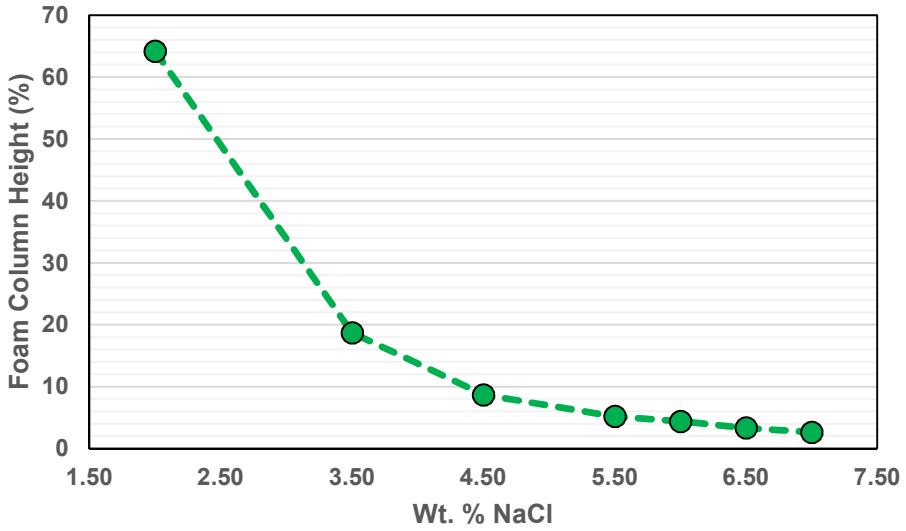

Fig. 5.5: Bulk dynamic foam stability results for undiluted samples.

The 2.0 wt. % NaCl case demonstrated a decrease of around 35% compared to the control case. As the salinity increased from 2.0 wt. % to 7.0 wt. %

NaCl within the Winsor Type I microemulsion region, the dynamic foam stability decreased more than 90.0%, as measured by equilibrium foam column height. The magnitude of foam stability reduction was monotonically decreasing with increasing salinity with the most dramatic change of ~70% coming between 2.0 wt. % and 3.5 wt. % NaCl. The salinity transition from 2.0 wt. % to 7.0 wt. % NaCl corresponded to increasing overall oil solubilization (0.93% to 3.92% concentration) and increasing micelle size (9.0 to 28.0 nm in diameter) due to decreasing repulsion between hydrophilic head groups of surfactant monomers (Rosen and Kunjappu 2012), which led to decreasing micelle concentration (Fig. 5.2). Lee *et al.* (2014, 2016) found that sodium dodecyl sulfate (SDS) solutions with solubilized n-dodecane resulted in less stable foam compared to oil-free solutions because oil solubilization reduced intramicellar repulsion. The impact of bulk microemulsion viscosity on film drainage was ruled out due to the fact that the dynamic foam stability decreases despite microemulsion viscosity remaining relatively constant with varying salinity (Table 5.1).

Therefore, the factors concerning oil-swollen micelles which directly impact foam stability were:

1) Decreasing micelle concentration with increasing salinity
2) Increasing micelle size with increasing salinity
3) Decreasing intramicellar repulsion with increasing oil solubilization

The ~70% decrease in foam stability from 2.0 wt. % NaCl to 3.5 wt. % NaCl (Fig. 5.5) corresponded to the 50.0% decrease in micelle concentration (Fig. 5.2) compounded with decreasing intramicellar repulsion and increasing micelle size. However, the ~50% decrease in foam stability from 3.5 wt. % to 4.5 wt. % NaCl corresponds to only an 8.2% decrease in micelle concentration, so in this range

the effects of decreased intramicellar repulsion and increased micelle size were more impactful. This indicated a nonlinear relationship between foam stability and each of the three factors listed above and that there might also be interaction between the factors themselves.

The dilution tests controlled oil-swollen micelle size while varying concentration to clarify the individual contributions of the factors listed above. Surface tension measurements showed no significant difference between diluted and undiluted samples, which allowed for continued analysis based on the action of oil-swollen micelles within the film rather than interfacial effects. The results shown in Fig. 5.6 demonstrate that for each fixed oil-swollen micelle size, diluting the sample reduces the foam stability.

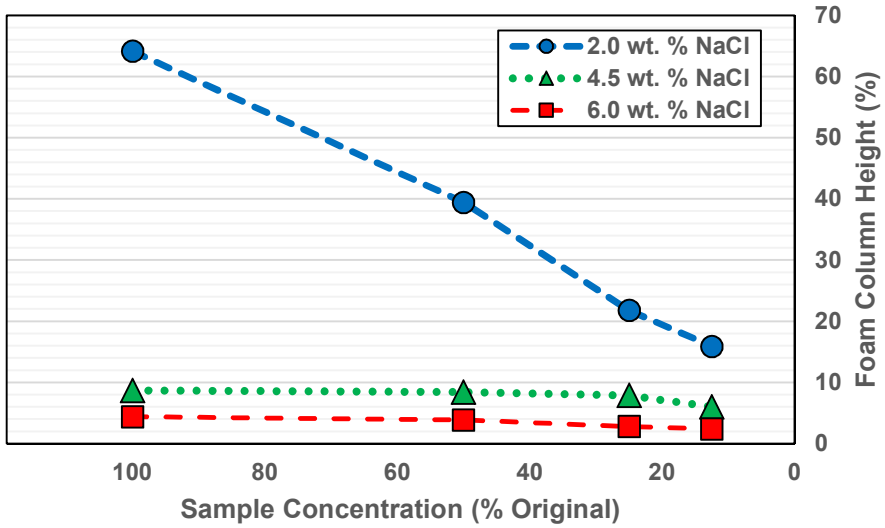

Fig. 5.6: Bulk dynamic foam stability results for diluted samples.

It should be noted that these dilutions (50.0%) at most resulted in a commensurate (50.0%) decrease in foam stability, and for most cases resulted in

less than 50.0% decrease in foam stability. This was because micellar structuring affects foam stability in a non-linear fashion (Wasan *et al.* 1988). The small changes in foam stability under dilution for 4.5 wt. % and 6.0 wt. % NaCl are due to the initially low micelle concentration in these samples, which would lead to less complex stratification and less penalty for dilution. Therefore, oil-swollen micelles exhibited less effective micellar structuring compared to oil-free micelles, but still contributed to a more stable foam by their presence rather than their absence.

5.3.3 Microfluidic Decay Testing

The transition to the porous media microfluidic model allowed for examination of foam stability in the presence of microemulsion in a much more confined and representative porous medium. In particular, the foam in the microfluidic model differed from bulk because it had two-dimensional connectivity of Laplace borders, was shaped by the porous medium, and was subject to higher capillary pressures due to the minute flow channels in the porous medium. In addition, the mode of testing was static decay rather than the dynamic mode of the Bikerman-style tests. The static decay test reproduced the phenomenon of foam decay in an enhanced oil recovery scenario far away from the injection well(s). In the far-field, mobile foam propagates slowly and a significant portion remains trapped. Comparing the trends of foam stability testing at different scales and by different methods allowed for confirmation of the impact of oil-swollen micelles on foam stability in a porous medium.

Both the undiluted (Fig. 5.7) and diluted (Fig 5.8) sample tests held to the general trend observed in the bulk foam stability testing, with foam stability

decreasing as sample salinity was increased from 2.0 wt. % to 7.0 wt. % NaCl and also as sample concentration decreased from 100.0% to 12.5%.

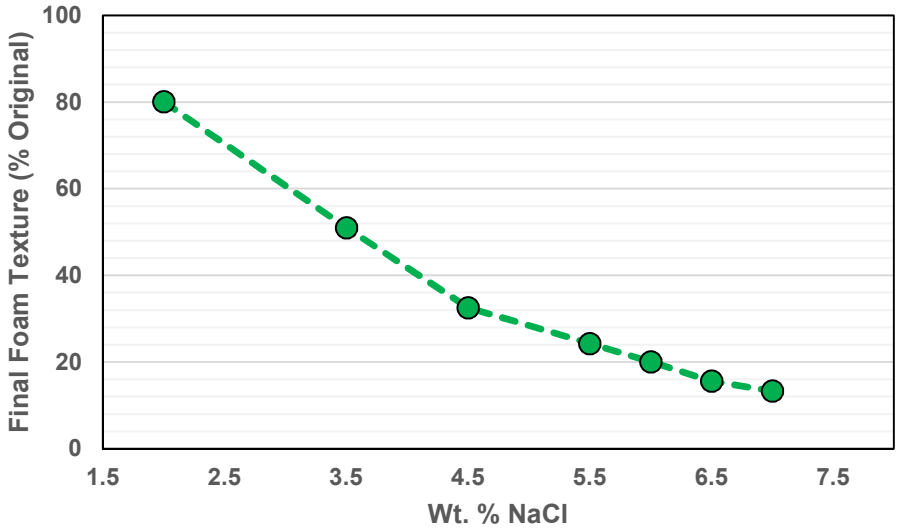

Fig. 5.7: Microfluidic static decay results for undiluted samples.

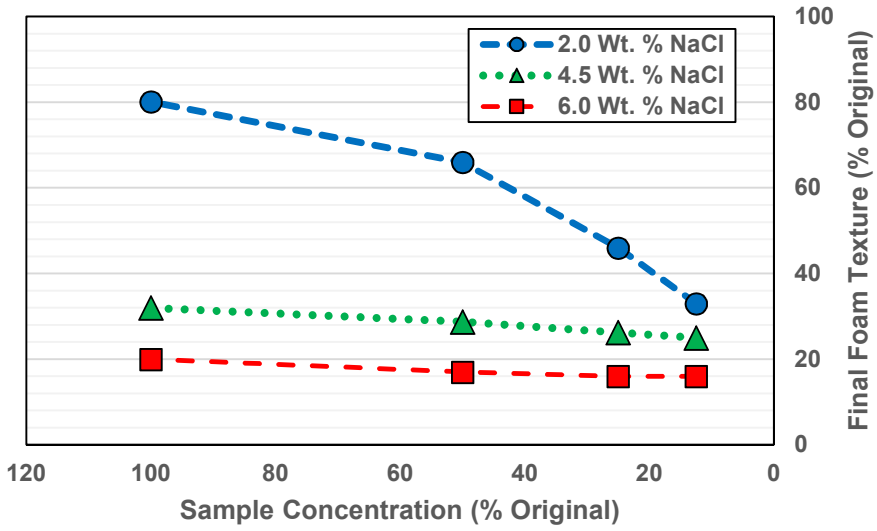

Fig. 5.8: Microfluidic static decay results for diluted samples.

The similarity in trends for both the undiluted and diluted samples at bulk and microfluidic scales improved confidence in the previous interpretation concerning microemulsion-foam interactions. It was noted that the relative importance of oil-swollen micelle concentration, micelle size, and intramicellar repulsion varied depending on the current state of each individual factor, confirming the presence of interaction effects at the porous medium scale in accordance with observations made at the bulk scale.

Reduced intramicellar repulsion with increasing salinity of Winsor Type I microemulsions led to less resistance to film thinning, but it was not immediately clear how larger, sparser micelles contributed to foam stability. Lee *et al*. (2014) have shown that as film thickness decreases, micellar structuring results in an ordered aggregation which resists film thinning and based on the current work, this viscosifying structure becomes less effective with larger, sparser oil-swollen micelles.

5.4 KEY FINDINGS

1) There is a significant impact of microemulsion phase behavior on foam stability, which resulted in up to ~95% and 85% decreases in bulk foam stability and confined porous medium foam static stability, respectively.
2) Foam stability decreased most significantly for the initial increase in salinity from 2.0 wt. % to 3.0 wt. % NaCl and then decreased more gradually as salinity was increased which indicates that large improvements in foam stability may be made by decreasing the salinity of the microemulsion phase behavior environment.

3) The decrease in foam stability was due to the action of oil-swollen micelles within liquid lamellae, which exhibited impaired micellar structuring as neutral electrolyte concentration increased due to reduced availability, increased size, and decreased intramicellar repulsion.
4) Results suggest that interaction between effects may be significant, i.e. the relationship between foam stability and a certain factor id dependent on the state of the other two factors as well.
5) Dilution testing showed that although oil-swollen micelles were not as effective as oil-free micelles in stabilizing foam, their presence still contributed to micellar structuring that resisted film drainage.
6) Free surfactant monomers exist and are available to aggregate at gas-liquid interfaces in equilibrium with oil-swollen micelles in Winsor Type I microemulsions and that this held true not only for the original 0.5 wt. % surfactant solutions, but even for the solutions with concentrations as low at 0.0625 wt. % under dilution.
7) Trapped foam stability exhibits sensitivity to microemulsion phase behavior similarly to bulk foam dynamic stability, which highlights the dynamic nature of trapped foam.
8) Both modes of testing showed similar trends, indicating that bulk foam dynamic stability testing may be an adequate routine screening procedure for foam stability in the presence of microemulsion for LTG processes.

Chapter 6: Summary and Recommendations

6.1 SUMMARY

The following is an executive summary of the preceding work. Detailed discussion and analysis are provided at the end of Chapters 4 and 5.

The LTG process is a close analogue to the surfactant-polymer process, but it replaces polymer with aqueous foams for liquid mobility control and thus extends applicability to challenging oil reservoir conditions such as high salinity, high temperature, and low permeability. Low Tension Gas flooding, like most surfactant EOR processes, is typically designed with a salinity gradient to improve surfactant transport and maximize pure oil recovery. This work addressed the impact of salinity gradient design on Low Tension Gas flooding performance through a combination modeling/simulation and experimental study.

6.1.1 LTG Model Development and Validation with Salinity Gradient Study – Chapters 3 and 4

A streamlined LTG model was first developed in order to enhance experimental interpretation of LTG corefloods and improve theoretical understanding of the LTG process. Modeling was split into microemulsion and foam modeling, and existing state-of-the-art approaches were reviewed.

A simplified microemulsion model was developed based on the assumption that the middle phase microemulsion need not be modeled in a Winsor Type III environment due to the minimal volume of the middle phase and the fact that it ought to transport with oil and water in an ultra-low IFT environment. This reduces the maximum number of phases from three to two and removes the uncertainty of microemulsion phase properties such as relative permeability and capillary desaturation.

The simplified microemulsion model thus relies on a reduced set of readily available experimental data and focuses on the end effect of oil-water relative permeability alteration. This model was coupled with an empirical foam model that likewise minimizes parameters in favor of focusing on end effects. A detailed description of the complete model development and implementation is provided in Chapter 3.

A coreflooding study was performed with moderate permeability Berea sandstone to investigate the impact of salinity gradient on LTG flooding performance and also to validate the newly developed LTG model. The addition of foam mobility control to surfactant flooding (from LTG #1 to LTG #2) resulted in an approximately 58% increase in ROIP recovery as well as reduced dispersive mixing and surfactant adsorption. However, an elongated oil bank in LTG #2 indicated a loss of mobility control and room for improvement in salinity gradient design.

Reducing the slug salinity from optimum to the boundary between Winsor Type III and Winsor Type I regimes resulted in slower oil breakthrough, but nearly 15% ROIP recovery increase along with further reductions in dispersive mixing and surfactant adsorption. This was due to the fact that reducing slug salinity below optimum salinity resulted in less Type III behavior and oil mobilization, but more effective displacement of mobilized oil due to stronger foam mobility control (evidenced by 30% higher mobility reduction and gas trapping in the presence of foam). This was shown to possibly be due to the impact of microemulsion phase behavior on foam stability, which was investigated in the subsequent study.

6.1.2 Further Investigation of Microemulsion-Foam Interactions – Chapter 5

In order shed light on the impact of microemulsion phase behavior on foam stability, a multi-scale foam stability experiment was performed using Bikerman-style dynamic foam testing at the bulk scale and microfluidic static decay testing at the porous medium scale. This study was confined to the Winsor Type I microemulsion regime because of its ready analogy to oil-free micelles.

Size and concentration measurements were first performed and showed that oil-swollen micelles increase in size and decrease in concentration with increasing salinity. Surface tension measurements were also performed to rule out the impact of oil-swollen micelles on surfactant adsorption at the air-liquid interface, and the results showed that oil-swollen micelles did not significantly decrease surfactant adsorption compared to the oil-free case. This allowed for analysis of the foam stability tests in terms of the action of oil-swollen micelles within lamellae alone.

Bulk and porous medium foam testing showed up to 90% decrease in foam stability with similar trends at both scales as oil-swollen micelle diameter increased from 9.30 to 27.08 nm and concentration decreased over 80%. The decrease in micelle availability and micellar structuring effectiveness explain the impact of microemulsion phase behavior on foam stability.

The microfluidic static decay tests highlight the evolution of trapped foams that would likely be found in the far-field in foam processes and demonstrate the need for dynamic gas trapping modeling in the presence of foam.

6.2 Recommendations for Future Work

Although this work provides a foundation for analyzing the impact of salinity gradient on LTG performance, studies need to be performed under varying

conditions to better understand how the optimal balance of ultra-low IFT, foam mobility control, and surfactant transport change in problem-specific ways. In particular, work needs to be done to translate these findings from the moderate permeability to the low/ultralow permeability regimes that are the desired targets for the LTG process. In addition, carbonate reservoirs pose unique salinity gradient design challenges that have already been investigated in part (Das et *al.* 2016), but not yet systematically.

This work also highlighted the importance of gas trapping in the presence of foam for liquid mobility control in the LTG process, although the model used in the simulation study is rudimentary and not representative of the dynamic nature of gas trapping. Further insight could be provided via a computed-tomography (CT) scan study so that in-situ gas saturation evolution could be tracked. Addition of radioactive tracers would allow for quantification of trapped gas as in the work done by Nguyen (2009).

Results from an experimental gas trapping study would also be highly beneficial in improving the streamlined LTG model, either by tuning existing approaches such as the mechanistic model proposed by Balan (2013) or by developing a new analytical correlation altogether.

References

Azam, M.R., Tan, I. M., Ismail, L., Mushtaq, M., Nadeem, M., Sagir, M., "Static adsorption of anionic surfactant onto crushed Berea sandstone", *Journal of Petroleum Exploration and Production Technology* 3: 195-201, April 2013.

Balan, H.O., "Dynamics of Foam Mobility in Porous Media", Dissertation, The University of Texas at Austin, May 2013.

Bardon, C. and Longeron, D.G., "Influence of Very Low Interfacial Tensions on Relative Permeability", SPE 7609 presented at the SPE 53rd Annual Fall Technical Conference and Exhibition, Houston, Texas, 1-4 October 1978.

Bretherton, F.P., "The motion of long bubbles in tubes", *Journal of Fluid Mechanics* 10 (2): 166-188, March 1961.

Chambers, K.T. and Radke, C.J., *Interfacial Phenomena in Petroleum Recovery*, Marcel Dekker: New York, 1991.

Cottin, C., Morel, D., Levitt, D., Cordelier, P., and Pope, G., "Alkali surfactant gas injection: Attractive laboratory results under the harsh salinity and temperature conditions of middle east carbonates", *Abu Dhabi International Petroleum Exhibition and Conference 2012, ADIPEC 2012 – Sustainable Energy Growth: People, Responsibility, and Innovation* 4: 2542-2554, November 2012.

Das, A., Nguyen, N., Alkindi, A., Farajzadeh, R., Southwick, J., Vincent-Bonnieu, S., and Nguyen, Q.P., "Low Tension Gas Process in High Salinity and Low Permeability Reservoirs," SPE 179839 presented at the SPE EOR Conference at Oil and Gas West Asia held in Muscat, Oman, 21–23 March 2016.

Delshad, M. Bhuyan, D., Pope, G.A., and Lake L.W., "Effect of Capillary Number on the Residual Saturation of a Three-Phase Micellar Solution", SPE 14911 presented at the SPE Enhanced Oil Recovery Symposium, Tulsa, Oklahoma, 20-23 April 1986.

Derjaguin, B.V. and Obukhov, E.V., *Acta Physiochim. URSS*, 1936.

Derjaguin, B.V. and Obukhov, E.V., *Acta Physiochim. URSS*, 1939.

Derjaguin, B. and Landau, L., "Theory of the stability of strongly charged lyophobic sols and of the adhesion of strongly charged particles in solution of electrolytes.", *Acta Physiochim. URSS* 14: 633-662, 1941.

Friedmann, F., Chen, W.H., and Gauglitz, P.A., “Experimental and Simulation Study of High-Temperature Foam Displacement in Porous Media.” *SPE Reservoir Eval. Eng.* 6 (1): 37-45, February 1991.

Green, D.W. and Willhite, G.P., *Enhanced Oil Recovery*, SPE, 1998.

Gupta, S. P, and Trushenski, S. P., “Micellar Flooding – Compositional Effects on Oil Displacement”, *SPEJ* 19 (2): 116-128, April 1979.

Hand, D.B., “Dineric Distribution: I. The Distribution of a Consolute Liquid Between Two Immiscible Liquids”, *Journal of Physics and Chemistry* 34: 1961-2000, 1930.

Harbert, L.W., “Low Interfacial Tension Relative Permeability”, SPE 12171 presented at the 58th Annual Technical Conference and Exhibition, San Francisco, California, 5-8 October 1983.

Healy, R.N. and Reed, R.L., “Immiscible Microemulsion Flooding”, *SPEJ* 17(02): 129-139, April 1977.

Hirasaki, G. J., van Domselaar, H. R., and Nelson, R. C. “Evaluation of the Salinity Gradient Concept in Surfactant Flooding”, *SPEJ* 23 (03): 486-500, June 1983.

Hirasaki, G.J. and Lawson, J.B., “Mechanisms of Foam Flow in Porous Media: Apparent Viscosity in Smooth Capillaries”, *SPEJ* 25(02): 176-190, April 1985.

Huh, C., “Interfacial tensions and solubilizing ability of a microemulsion phase that coexists with oil and brine”, *Journal of Colloid and Interface Science* 71 (2): 408-426, September 1979.

Kam, S.I., Nguyen, Q.P., Li, Q., Rossen, W.R., “Dynamic Simulations With an Improved Model for Foam Generation”, SPE 90938 presented at the SPE Annual Technical Conference and Exhibition, Houston, Texas, 26-29 September 2004.

Kil, R.A., Nguyen, Q.P., and Rossen, W.R., “Determining Trapped Gas in Foam From Computed-Tomography Images.” *SPEJ* 16 (01): 24-34, March 2011.

Kovscek, A.R. and Radke, C.J., *Fundamentals of Foam Transport in Porous Media*, University of California, Berkeley, October 1993.

Kovscek, A.R., Patzek, T.W., and Radke C.J., “A mechanistic population balance model for transient and stead-state foam flow in Boise sandstone”, *Chemical Engineering Science* 50 (23): 3783-3799, December 1995.

Lee, J., Nikolov, A., and Wasan, D., “Stability of Aqueous Foams in the Presence of Oil: On the Importance of Dispersed vs Solubilized Oil”, *Ind. & Eng. Chem. Res.* 52: 66-72, 2013.

Lee, J., Nikolov, A., and Wasan, D., “Surfactant micelles containing solubilized oil decrease foam film thickness stability”, *Journal of Colloid and Interface Science* 415: 18-25, October 2014.

Lee, J., Nikolov A.D., and Wasan, D.T., “Stepwise thinning dynamics of a foam film formed from an anionic micellar solution”, *Journal of Colloid and Interface Science* 487: 214-222, October 2016.

Mysels, K.J. and Otter, R.J., “Conductivity of mixed sodium decyl and dodecyl sulfates—the composition of mixed micelles”, *Journal of Colloid Science* 16 (5): 462-473, October 1961.

Mysels, K.J. and Otter, R.J., “Thermodynamic aspects of mixed micelles—application to an empirically established equilibrium”, *Journal of Colloid Science* 16 (5): 474-480, October 1961.

Nelson, R. C and Pope, G. A., “Phase Relationship in Chemical Flooding”, *SPEJ* 18(5): 325-338, October 1978.

Nguyen, N., Nguyen, Q.P., Ren, G., Mateen, K., Cordelier, P.R., Morel, D.C., "Low-Tension Gas (LTG) Injection Strategy in High Salinity and High Temperature Sandstone Reservoirs," SPE 174690 presented at the SPE Asia Pacific Enhanced Oil Recovery Conference, Kuala Lumpur, Malaysia, 11–13 August 2015.

Nguyen, Q.P., Zitha, P.L.J., Currie, P.K., and Rossen, W.R., “CT Study of Liquid Diversion With Foam”, *SPE Production & Operations* 24 (01): 12-21, February 2009.

Nikolov, A.D., Wasan, D.T., Huang, D.W., Edwards, D.A., “The Effect of Oil on Foam Stability: Mechanisms and Implications for Oil Displacement by Foam in Porous Media”, SPE 15443 presented at the SPE Annual Technical Conference and Exhibition, New Orleans, Louisiana, 5-8 October 1986.

Nikolov, A.D. and Wasan, D.T., “Ordered Micelle Structuring in Thin Films Formed from Anionic Surfactant Solutions: I. Experimental”, *Journal of Colloid and Interface Science* 133 (1): 1-12, November 1989.

Noll, L.A and Gall, B.L., “Flow adsorption calorimetry of surfactants as a function of temperature, salinity, and wettability”, *Colloids and Surfaces* 54: 41-60, 1991.

Patzek, T.W., “Description of Foam Flow in Porous Media by the Population Balance Method”, *Surfactant-Based Mobility Control*, Chapter 16: 326-341, July 1988.

Pope, G.A. and Nelson, R.C., “A Chemical Flooding Compositional Simulator”, *SPEJ* 18 (05): 339-354, October 1978.

Radke, C.J., and Gillis, J.V., “A Dual Tracer Technique for Determining Trapped Gas Saturation during Steady Foam Flow in Porous Media”, SPE 20519 presented at the SPE Annual Technical Conference and Exhibition, New Orleans, LA, 23-26 September 1990.

Ronde, H., “Relative Permeability at Low Interfacial Tensions”, SPE 24877 presented at the 67th SPE Annual Technical Conference and Exhibition, Washington, D.C., 4-7 October 1992.

Roof, J.G., “Snap-Off of Oil Droplets in Water-Wet Pores”, *SPEJ* 10 (01): 85-90, March 1970.

Rosen, M.J. and Kunjappu, J.T., *Surfactants and Interfacial Phenomena, Fourth Edition,* John Wiley & Sons, Inc., 9 January 2012.

Ross, S.J. and Bramfitt, T.H., “Inhibition of Foaming. VIII. Changes in Electrical Conductivity of Colloidal Electrolyte Solutions on Addition of Non-ionic Foam Stabilizers and Foam Inhibitors”, *The Journal of Physical Chemistry* 61 (10): 1261-1265, 18 October 1957.

Shah, D.O., Oh, S.G., and Huibers, P.D.T. 1996, “Pressure-Jump Studies on Micellar Relaxation Time and its Effect on Various Technological Processes”, *Surfactants in Solution*, Marcel Dekker, Inc., New York, NY.

Srivastava, M, “Foam Assisted Low Interfacial Tension Enhanced Oil Recovery Process”, Dissertation, University of Texas at Austin, 2010.

Srivastava, M. and Nguyen, Q.P., “Application of Gas for Mobility Control in Chemical EOR in Problematic Carbonate Reservoirs,” SPE 129840 presented at the 2010 SPE Improved Oil Recovery Symposium, Tulsa, Oklahoma, 24–28 April 2010.

Szlendak, S. M., Nguyen, N., and Nguyen, Q. P. “Laboratory Investigation of Low-Tension-Gas Flooding for Improved Oil Recoveries in Tight Formations”, *SPEJ* 18 (5): 851-866, August 2013.

Szlendak, S.M., Nguyen, N., Nguyen, Q.P., “Investigation of Localized Displacement Phenomenon for Low-Tension-Gas (LTG) Injection in Tight

Formations," *Journal of Petroleum Science and Engineering* 142: 36-45, June 2016.

Schramm, L.L. 1994. *Foams: Fundamentals & Applications in the Petroleum Industry,* ACS Advances in Chemistry Series 242, American Chemical Society, Washington, DC.

Sheng, J. J., *Modern Chemical Enhanced Oil Recovery*, Gulf Professional Publishing, 2011.

Tang, G.Q., and Kovscek, A.R., "Trapped Gas Fraction During Steady-State Foam Flow", *Transport in Porous Media* 65 (2): 287-307, November 2006.

Verwey, E.J.W., and Overbeek, J.Th.G., *Theory of the Stability of Lyophobic Colloids*, Elsevier: New York, 1948.

Wasan, D.T., Koczo, K., and Nikolov A.D., "Mechanisms of Aqueous Foam Stability and Antifoaming Action with and without Oil: a Thin-Film Approach", *Advances in Chemistry* 242: 47-114, July 1988.